Title: Compound Drivers of Antarctic Sea Ice Loss

Author Information

Aditya Narayanan[1] (adityarn@gmail.com), Holly Ayres[2](holly.ayres@noc.ac.uk), Matthew H. England[3] (m.england@unsw.edu.au), F. Alexander Haumann[4,5] (alexander.haumann@awi.de), Matthew R. Mazloff[6] (mmazloff@ucsd.edu), Alessandro Silvano[1] (a.silvano@soton.ac.uk), Theo Spira[4,7] (theo.spira@awi.de), Shenjie Zhou[8] (shezhou@bas.ac.uk), Alberto C. Naveira Garabato[1] (acng@soton.ac.uk)

[1]Ocean and Earth Science, University of Southampton, U.K.

[2]National Oceanography Centre, U.K.

[3]Center for Marine Science and Innovation, and ARC Australian Centre for Excellence in Antarctic Science, University of New South Wales, Australia

[4]Alfred Wegener Institute, Helmholtz Centre for Polar and Marine Research, Bremerhaven, Germany

[5]Ludwig-Maximilians-Universität München, Munich, Germany

[6]Scripps Institution of Oceanography, University of California San Diego

[7]Department of Marine Science, University of Gothenburg, Sweden

[8]British Antarctic Survey, U.K.

Compound Drivers of Antarctic Sea Ice Loss

Aditya Narayanan[1*], Holly Ayres[2], Matthew H. England[3],
F. Alexander Haumann[4,5], Matthew R. Mazloff[6], Alessandro Silvano[1],
Theo Spira[7], Shenjie Zhou[8], Alberto C. Naveira Garabato[1]

[1]Ocean and Earth Science, University of Southampton, U.K.
[2]National Oceanography Centre, U.K.
[3]Center for Marine Science and Innovation,
and ARC Australian Centre for Excellence in Antarctic Science,
University of New South Wales, Australia
[4]Alfred Wegener Institute, Helmholtz Centre for Polar and Marine Research,
Bremerhaven, Germany
[5]Ludwig-Maximilians-Universität München, Munich, Germany
[6]Scripps Institution of Oceanography, University of California San Diego
[7]Department of Marine Science, University of Gothenburg, Sweden
[8]British Antarctic Survey, U.K.

*To whom correspondence should be addressed; E-mail: a.narayanan@soton.ac.uk.

Antarctic sea-ice extent began declining since 2015, reaching its lowest extent in the post-1970s observational era in 2023. To diagnose the drivers of this decline, we analyse an observationally constrained sea ice-ocean model spanning 2013-2023, and identify three distinct phases of sea-ice retreat. First, an intensification of westerly winds preconditioned the Southern Ocean via increased upwelling of warm, saline Circumpolar Deep Water (CDW). Second, strong winds in 2015 and 2016 enhanced the mixing of CDW into the upper ocean and thus initiated sea-ice loss, particularly in East Antarctica. Third, sustained mixing of CDW into the surface layer combined with reduced equatorward freshwater export maintained an unprecedented low sea-ice state. East Antarctic sea-ice loss was primarily subsurface-driven, whereas West Antarctic loss was also forced by cloud-mediated longwave radiative flux anomalies. Our findings suggest that persistent upwelling-favourable conditions under anthropogenic forcing may push the Southern Ocean into a prolonged low sea-ice state.

Short Title

Compound Drivers of Antarctic Sea Ice Loss.

One Sentence Summary

Enhanced upwelling and mixing of heat and salt from the subsurface ocean has driven the sustained loss of Antarctic sea ice since 2015.

1 Introduction

Antarctic sea ice is an important component of the global climate system, modulating the albedo of the Southern Ocean (*1*), the upper and lower branches of the meridional overturning circulation (*2*), the water mass transformations therein (*3*), oceanic heat and carbon uptake (*4*), ocean heat content (*5*), and biological productivity (*6*).

Antarctic sea ice exhibited a slight positive trend from 1979 to 2015 (*7–9*), with large regional variations. The expansion of sea ice over this period was most likely associated with an increased wind-driven northward transport of sea ice (*10*) and a resulting surface freshening due to the export of freshwater via sea ice from the high-latitude Southern Ocean (*11*). However, since 2015, the observed sea ice area has experienced persistent negative anomalies, with the lowest wintertime and summertime sea ice extents measured in 2023 (*12*). The negative sea ice extent anomalies were associated with heightened temperatures in the upper 100 m of the water column (*13*) and elevated surface salinity (*14*). This rapid change in Southern Ocean sea ice from record-high to record-low anomalies is one of the largest present-day climatic shifts in the Earth system, and has the potential to accelerate planetary warming (*1*) and to disrupt the conventional pathways for heat and carbon sequestration in the Southern Ocean (*15*). In addition, sea ice loss has the potential to adversely impact the ecosystem (*16*).

Several hypotheses have been proposed to explain the roles of the ocean and atmosphere in modulating the recent reduction of Antarctic sea ice extent. Revisiting these hypotheses by categorizing them based on the timescales of the proposed mechanisms can provide valuable insight. On synoptic timescales, wind variations can immediately influence the ocean's Ekman advection. For example, during the summers of 2016/17 and 2019/20, a sudden weakening of the westerlies resulted in reduced northward Ekman advection of relatively cool and fresh surface waters, leading to surface warming and salinification in the offshore subpolar Southern Ocean (*17*). This warming may have contributed to the summertime reduction in sea ice area and subsequent delayed sea ice growth. On seasonal timescales, intense polar cyclones were likely linked to the formation of open-ocean polynyas in the Weddell Sea in 2016 and 2017 (*18–20*). Additionally, a positive Zonal Wave-3 (ZW3) pattern (*21*) during 2016 was associated with stronger poleward transport of warm subtropical air masses, enhancing cloud cover over the sea ice field and downward longwave radiative fluxes (*18, 22*). Warm northerly air flow was linked to a deepening of the Amundsen Sea Low (ASL)in 2016 and 2019 (*20, 23*). The spatio-temporal trajectory of the ZW3 pattern in 2016 influenced sea ice concentration and drift, contributing to reduced sea ice extent in the Weddell Sea, the Amundsen and Bellingshausen Seas, and the western Ross Sea (*22, 24–26*).

On seasonal to interdecadal timescales, the Southern Annular Mode (SAM) is the dominant mode of climate variability over the high-latitude regions of the Southern Ocean (*27*). A positive phase of the SAM is associated with a poleward shift and increased intensity of the westerlies, which regulate the rate of Ekman advection. An intensified SAM is thus expected to exert two opposing effects on upper-ocean stratification: surface freshening due to enhanced equatorward export of polar waters and sea ice (*28*), and surface salinification further south due to increased Ekman pumping (*29*). The SAM has trended positive since the 1970s (*27*), entailing an enhancement in the cyclonicity of winds over the subpolar Southern Ocean that have increased Ekman pumping of warm deep waters from the subsurface (*24, 30, 31*). Further, the SAM has exhibited increasing zonal asymmetry due to a deepening of the ASL and an intensification of the ZW3 pattern (*32*), which enhanced the poleward flow of warm, humid subtropical air masses within specific sectors of the Southern Ocean. Preindustrial runs of climate models show that the SAM–ZW3 interaction impacts the regional variability of sea ice (*33*).

Future sea ice evolution is likely to be governed by a balance between competing mechanisms. For example, the heat content in the ocean and atmosphere is expected to continue to increase under anthropogenic forcing, which would inhibit sea ice growth. In contrast, enhanced surface freshening (*34*) due to increased precipitation (*35*) and meltwater runoff (*36*) is expected to stratify the upper ocean and cause a slowdown in the abyssal overturning cell (*37, 38*), which would promote sea ice growth by inhibiting the vertical mixing of heat. However, in the present-day Southern Ocean, a somewhat surprising trend of upper-ocean salinification is occurring (*14*). This salinification acts to weaken stratification (*14*), potentially enabling the mixing of heat and salt from the subsurface Circumpolar Deep Water (CDW) layer (*39*).

The possible role of increased westerly winds in determining the fate of Antarctic sea ice was highlighted by a hypothesis within the literature, founded on idealized model studies. In this view, poleward intensifying westerlies would elicit a two-timescale response from the ocean (hereafter referred to as the two-timescale hypothesis) (*40*). The immediate response would involve enhanced northward Ekman transport of cooler and fresher waters from the high-latitude Southern Ocean, inducing surface cooling and enhanced sea ice cover. The delayed response would be associated with enhanced upward Ekman pumping of warm and saline CDW, bringing about a warmer and saltier upper ocean with reduced sea ice cover. However, the observed ocean response is more complex, influenced also by changes in surface fluxes associated with variability in the hydrological cycle. Recent, more realistic simulations further suggest that reduced sea ice extent can result from upwelling-favorable conditions arising either from natural Southern Ocean variability (*41*) or from historically forced conditions (*42*). Overall, the observed pattern of a gradual increase followed by an abrupt reduction in Antarctic sea ice cover after 2015 qualitatively aligns with expectations from the two-timescale hypothesis (*13*), though important differences remain.

While many potentially important processes have been proposed, the mechanisms governing the recent climatic evolution of Antarctic sea ice remain uncertain, and are the focus of vigorous scientific debate. Climate models generally struggle to represent the observed variability, and often simulate physically implausible scenarios (*43*). Here, we use an eddy-permitting, data-assimilative sea ice-ocean state estimate—the Biogeochemical Southern Ocean State Estimate (SOSE) (*44*)—to elucidate the drivers of Antarctic sea ice changes between 2013 and 2023, a period encompassing the point of abrupt reduction in ice cover. By constructing budgets of sea ice volume and conserved upper-ocean properties (such as heat and salt), we are able to identify the key factors in sea ice loss, and assess its forcing mechanisms and underpinning sequence of causal events.

Our analysis shows that the recent Antarctic sea ice loss was the compound outcome of three driving phases. First, prior to mid 2015, sea ice extent increased in association with cool and fresh anomalies in the upper ocean. Second, after mid 2015, heat and salt accumulated in the upper ocean, initially as a result of the shoaling of warm and saline CDW. This response, qualitatively consistent with the two-timescale hypothesis, was facilitated by upwelling-favourable winds and by enhanced vertical mixing of heat and salt, itself driven by intensified westerly winds. Then, in a third phase, the preceding sea ice changes altered surface freshwater fluxes, which became increasingly important in sustaining elevated salinity and weakened stratification in the upper ocean after 2018—thus promoting the persistence of a reduced Antarctic sea ice state.

Finally, we reveal substantial differences in the sea ice evolution and its driving mechanisms between East vs. West Antarctica. This zonal asymmetry stems from corresponding contrasts in wind forcing, highlighting the spatial complexity of Southern Ocean coupled atmosphere-ice-ocean dynamics. By identifying the dominant mechanisms within each region, we provide an integrated picture of circumpolar Antarctic sea ice changes.

2 Results

2.1 Overview of Southern Ocean hydrographic evolution

In the subpolar Southern Ocean, CDW lies just below the pycnocline in weakly stratified waters during winter (*45*). Relative to surface waters, CDW is characterized by warmer and saltier waters with lower concentrations of dissolved oxygen (DO) and higher concentrations of dissolved inorganic carbon (DIC) (*46*).

The off-shelf regions of East Antarctica (E Ant; between longitudes 60ºW and 150ºE; see Methods) exhibit a subsurface (below 100 m) warm anomaly and a surface cool and fresh anomaly during the years 2013-2016. Subsequently, the upper ocean (upper 100 m) becomes warmer and saltier, while the subsurface ocean cools and becomes slightly fresher (Figure 1A and 1B). This surface warming and salinification are accompanied by a depletion in DO (yellow contours in Figure 1A) and an increase in DIC (black contours in Figure 1B) in the upper ocean.

In West Antarctica (W Ant; between longitudes 150ºE and 60ºW; see Methods), the upper ocean exhibits a cool anomaly from 2013 to 2015, a warm anomaly from 2016 to 2020, and another cool anomaly from 2021 to 2023 (Figure 1C). The upper ocean shows DO depletion from 2013 to 2019 (yellow contours; Figure 1C). The subsurface ocean displays DO enrichment between 2017 and 2021 (black contours; Figure 1C). The upper ocean exhibits a salty anomaly from 2013 to 2019 (Figure 1D), with DIC enrichment observed from 2015 to 2019 (black contours; Figure 1D). After 2020, the upper ocean transitions to a fresh anomaly.

To summarise, beginning in mid-2015, the upper ocean off E Ant undergoes a clear transition from cooler, fresher, DO-enriched and DIC-depleted waters to a warmer, saltier, DO-depleted and DIC-enriched state. These anomalous properties are characteristic of CDW (*46*), thereby indicating an increased presence of CDW in the near-surface ocean, which is consistent

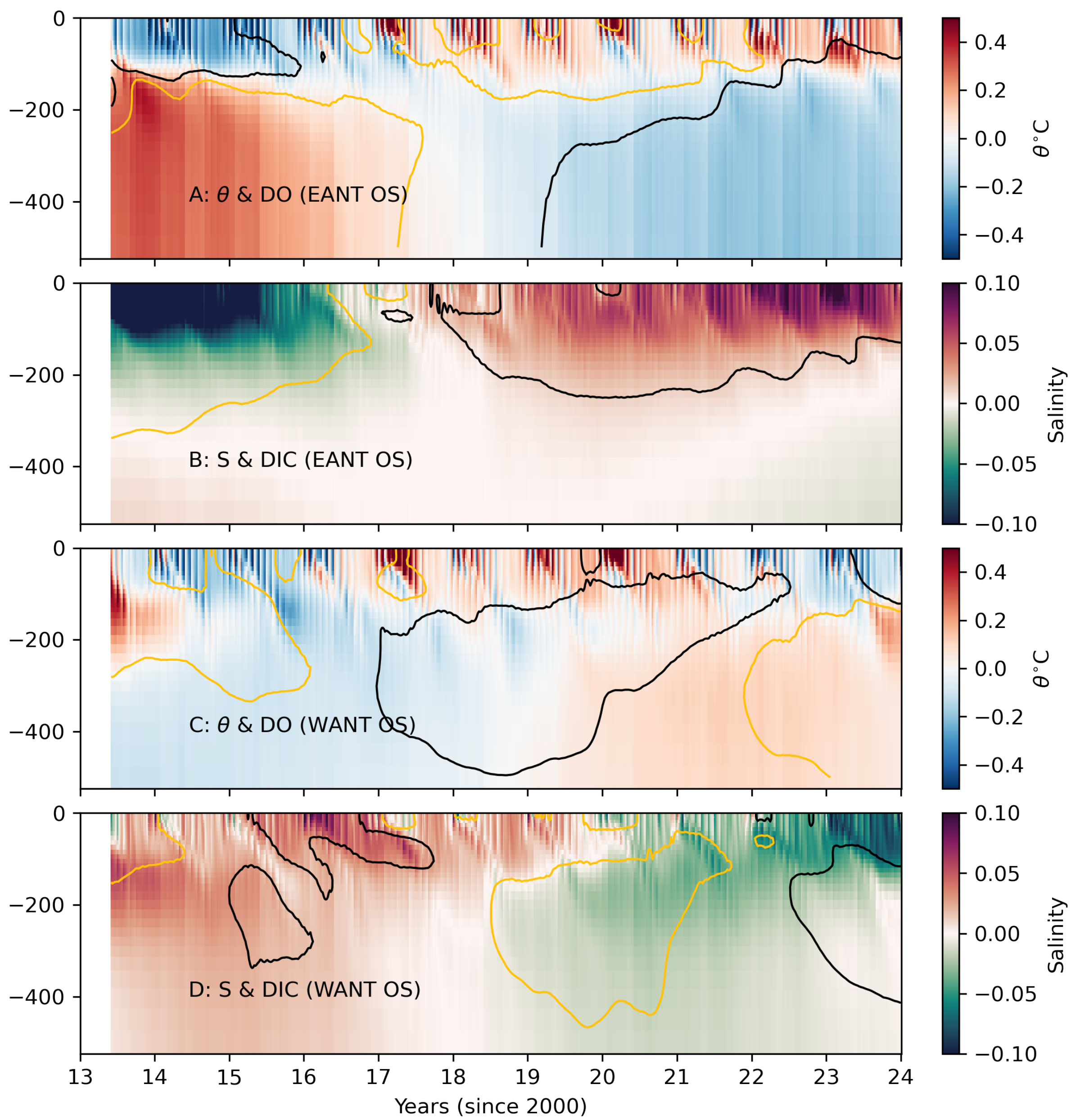

Figure 1: **SOSE hydrography.** SOSE potential temperature and salinity anomalies in (**A-B**) East Antarctica's off-shelf (EANT OS) and (**C-D**) West Antarctica's off-shelf (W Ant OS) regions. Contour lines in the temperature panels represent dissolved oxygen (DO) anomalies ($\pm 2\ \mu$molO/m^3), while contour lines in the salinity panels represent dissolved inorganic carbon (DIC) anomalies ($\pm 2\ \mu$molC/m^3). Negative anomalies are indicated by yellow contours, and positive anomalies are shown with black contours.

with observations (*31*). In contrast, the hydrographic evolution off W Ant appears more complex. While there is a clear transition from a saltier upper ocean (2013–2019) to a fresher upper ocean (2020–2023), the other parameters exhibit more convoluted changes.

The upper-ocean warming and salinification in association with sea ice loss seen in SOSE is consistent with studies based on in situ hydrographic profiles (*13*) and remotely sensed sea surface salinity (*14*). Here, we show that there is a zonal asymmetry in the evolution of upper-ocean hydrographic properties. Further, the mechanisms behind these changes have not yet been explored. In the following sections, we will consider budgets of sea ice volume, temperature and salinity to gain greater clarity on the dynamics governing the variability in Antarctic sea ice.

2.2 Antarctic sea ice extent and volume anomalies

Satellite observations reveal that negative SIE anomalies persisted beyond 2016 in both E Ant and W Ant (Figure 2a). Earlier observations indicate relatively stable sea ice with a zonal see-saw pattern in sea ice anomalies between W Ant (Ross, Amundsen and Bellingshausen Seas; see Methods) and E Ant (all regions outside W Ant), characterized by oppositely-signed anomalies across these regions prior to 2008. SIE anomalies in SOSE align with satellite observations, exhibiting positive biases with respect to observations from 2013 to 2016 in E Ant and from 2022 to 2023 in W Ant. Additionally, the temporal tendency of anomalies in SOSE generally matches that observed in satellite data. SIE anomalies largely reflect anomalies at the equatorward margin of the sea ice pack, but sea ice thickness anomalies in SOSE show that sea ice was reduced well within the pack as well (Figure S2). Both E Ant and W Ant display negative sea ice volume anomalies after 2016, with the off-shelf W Ant sea ice showing a recovery beyond 2021 (Figure 2 B-E).

Budgets reveal that the loss in sea ice volume in the off-shelf (bathymetry deeper than 3,000 m) E Ant region was driven by a drop in net thermodynamic sea ice production (SIP; i.e., growth minus melt; Figure 2F). This signal is consistent with earlier studies that suggested that sea ice loss beyond 2015 was largely thermodynamically forced, rather than mechanically driven by advection or divergence (*47*). However, due to uncertainties in sea ice thickness measurements, earlier studies could not quantify the volume loss now made evident by these results. While sea ice advection and divergence (AD) partially offset the decline in SIP, this was insufficient for full compensation, resulting in a negative anomaly in sea ice volume in E Ant (Figure 2B). The

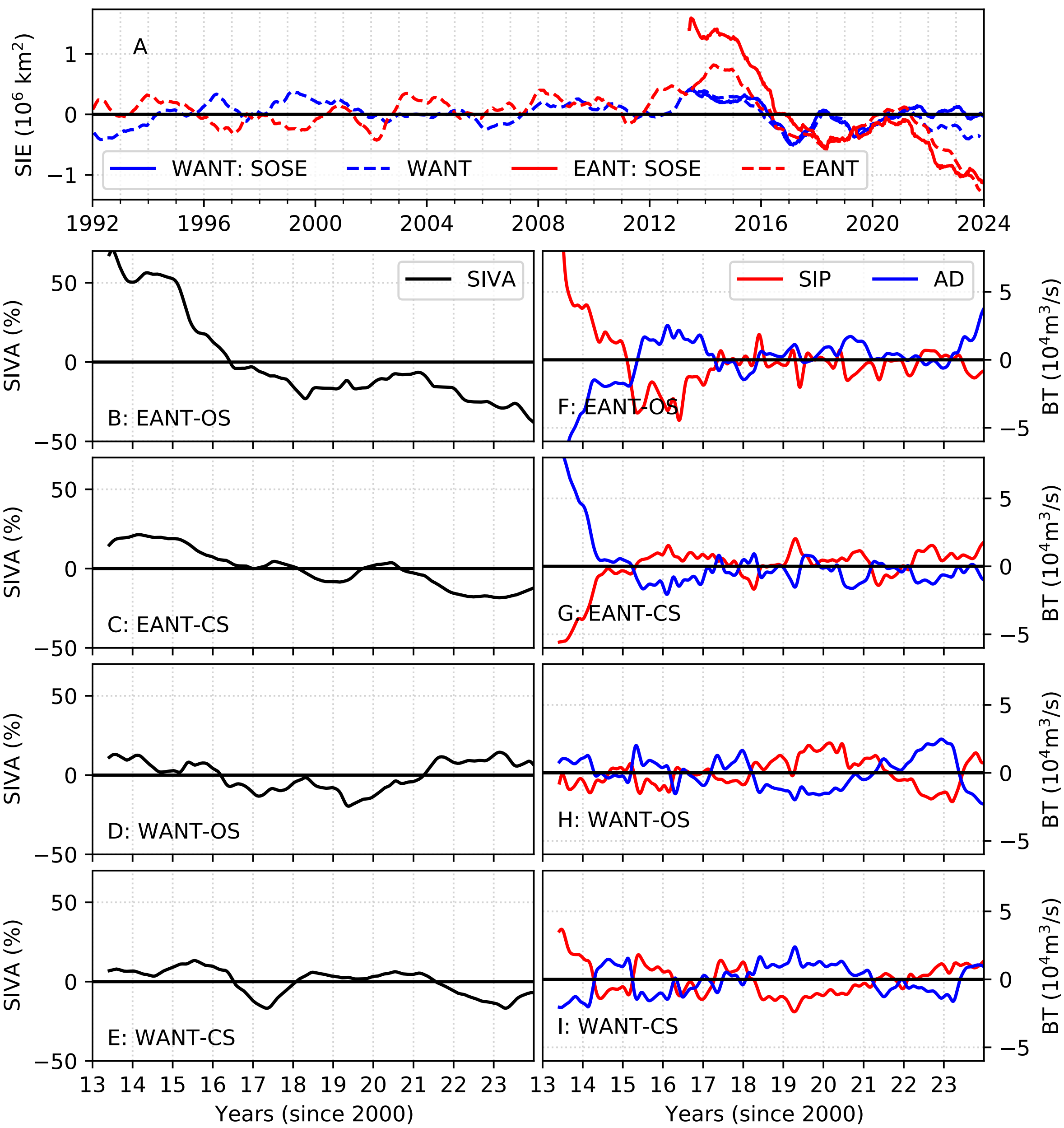

Figure 2: **Sea ice budgets.** (**A**) Sea ice extent anomalies computed from satellite observations (broken line) and SOSE (solid lines) for E Ant (EANT; red lines) and W Ant (WANT; blue lines). (**B-E.**) Sea ice volume anomalies (represented as percentage fraction of the monthly-mean volume), spatially summed over the continental shelf (CS) and off-shelf (OS) regions of East Ant and West Ant. (**F-I.**) Sea ice volume budget terms (BT) for the corresponding regions are shown on the right hand column. The terms, represented as anomalies, are the sea ice production (SIP; red line; computed as a residual of Equation 2) and the advection and divergence (AD; blue line) of sea ice volume.

additional contribution to sea ice from the AD term arises from enhanced sea ice production on the continental shelves of E Ant during 2015-2016, 2019-2020, and 2022-2023 (Figure 2G). This enhancement is likely due to increased sea ice export from the continental shelves, facilitated by reduced SIP in the off-shelf regions. A negative sea ice volume anomaly in both the continental shelf and off-shelf regions of E Ant was seen beyond 2020 (Figure 2F and 2G).

A negative sea ice volume anomaly is observed in both the off-shelf and continental shelf areas of W Ant (Figure 2D and 2E), though it is less pronounced than the sea ice loss in E Ant. The off-shelf region in W Ant shows a recovery in sea ice volume after 2021, but the continental shelf continues to exhibit a negative sea ice volume anomaly through 2023. Sea ice volume loss in the off-shelf region is primarily driven by low SIP during 2013–2017 and in 2022, while a negative anomaly in the AD term is evident during 2018–2020.

Budgets of sea ice volume in SOSE reveal a zonal asymmetry in sea ice evolution, with E Ant showing a persistent negative anomaly in sea ice volume beyond 2016 (Figure 2; EANT-OS and EANT-CS). In contrast, in W Ant, the loss in sea ice volume is not as pronounced, and does not last for the entire period beyond 2016 (Figure 2; WANT-OS and WANT-CS).

In the off-shelf W Ant region, SOSE sea ice volume exhibits a negative anomaly from 2016 to 2019, after which there is a recovery in sea ice. This recovery is also seen in satellite observations of SIE for a brief period in 2020 and 2021, but soon after there is once again a loss in SIE, not reproduced in SOSE. We discuss the reasons for this in later sections.

The sea ice volume budgets highlight the critical role of thermodynamics in reducing sea ice, suggesting that the mechanisms driving sea ice loss involve the transfer of heat to the ice. Heat can be sourced from the atmosphere above or from the warm CDW, typically found below the pycnocline. The sea ice loss was associated with a warming and salinification of the upper ocean along with an accumulation of DIC and a depletion of DO. Enhanced temperature, salinity and DIC, and reduced DO are the expected signatures of a greater near-surface presence of CDW (*48*). Thus, beyond 2016, upper-ocean properties are suggestive of intensified upward mixing of CDW.

In the large subpolar gyres of the Weddell and Ross Seas, the pycnocline (and underlying CDW layer) shoals to depths as shallow as 50–100 m (*31, 39, 45*). However, this heat remains trapped below the pycnocline unless stratification is sufficiently weakened to facilitate mixing of CDW into the surface mixed layer (*49, 50*). In cold polar waters, stratification is primarily controlled by salinity (*51*). To investigate the processes that lead to the weakening of stratification and the upward transfer of heat into the mixed layer, we analyse the upper-ocean temperature and salinity budgets in the next two sections.

2.3 Upper-Ocean warming in the Southern Ocean

Shortwave and longwave fluxes are primarily influenced by two factors: (1) sea ice, which alters surface albedo, and (2) cloud cover, which reduces the transmission of shortwave radiation through the atmosphere, but enhances downward longwave radiation. The subpolar Southern Ocean is generally characterised by a net heat loss via longwave radiation. Therefore, positive anomalies in longwave flux represent a reduction in this heat loss, effectively contributing to ocean warming.

Applying this framework to the off-shelf regions of E Ant, upper-ocean warming is evident from 2015 to 2018 (Figure 3A). Surface fluxes ("surf"; excludes shortwave fluxes) show positive anomalies (a warming tendency) during periods of expanded sea ice cover. This is consistent with the insulating effect of sea ice that suppresses heat loss to the atmosphere via longwave and sensible heat fluxes (years 2013-2014; red line in Figure 3E). After 2015, surface fluxes exhibit a prominent and sustained negative anomaly, reflecting greater heat loss to the atmosphere due to reduced sea ice cover (*12*) (surf; red line in Figure 3E).

Despite this shift, a key driver of upper-ocean warming beginning in 2015 is the vertical mixing term ($Diff_v$), which transitions from a negative to a sustained positive anomaly through 2023 (blue line in Figure 3E). In contrast, shortwave fluxes (SW; dashed red line in Figure 3E) only shift to a positive anomaly in mid-2016, following the onset of sea ice loss in mid-2015. This timing suggests that shortwave fluxes did not initiate the sea ice decline, but rather contributed to its subsequent intensification. Although surface fluxes acted to warm the ocean during 2013 and 2014, this warming was offset by cooling due to vertical mixing, resulting in little net temperature change. Starting in 2015, however, temperatures begin to rise (Figure 3A), initially driven by the intensification of vertical mixing.

The continental shelves of E Ant also exhibit a warming tendency, although this is slower and less pronounced than in the off-shelf regions (Figure 3B). The warming is initially driven by the vertical mixing term ($Diff_v$; Figure 3F). Surface fluxes (surf) align with changes in sea ice volume in this region (Figure 2C), exhibiting a warming tendency during phases of greater sea ice volume and a cooling tendency during periods of reduced sea ice volume. Shortwave fluxes display a prominent positive anomaly from 2021 to 2023, coinciding with substantial sea ice volume loss in these regions. Once again, a warming tendency via shortwave fluxes lags

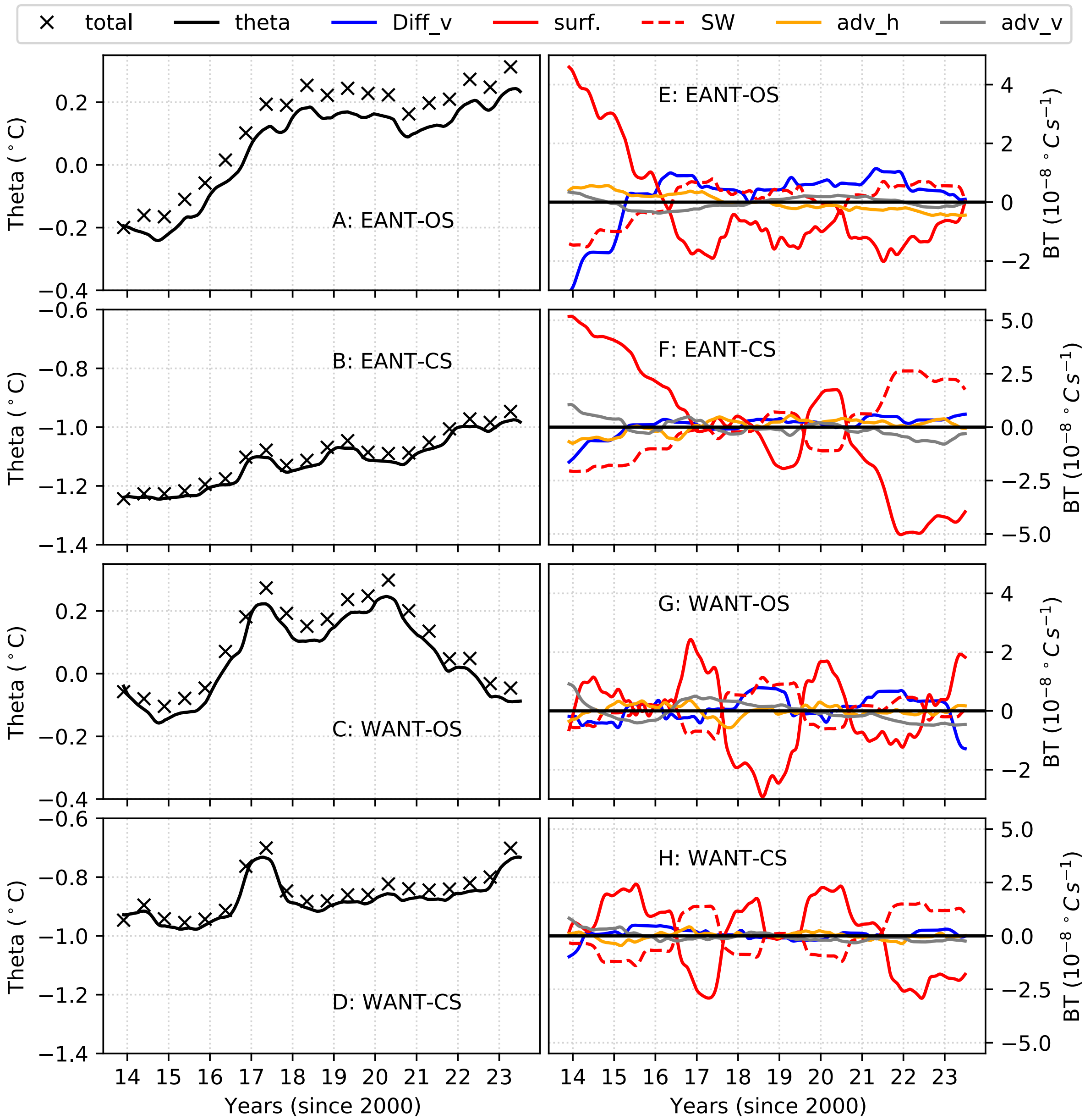

Figure 3: **SOSE temperature budget.** (**A-D.**) Potential temperature (θ; black line with cross markers), vertically averaged in the upper 100 m of the water column, and spatially averaged over the regions labeled within the panels. A 12-month rolling mean was applied to remove the seasonality. The time-integrated sum of the budget terms is shown by cross markers. (**E-H.**) θ budget terms are presented here as anomalies relative to their monthly means. Terms shown are the vertical advection (adv_v; grey lines), horizontal advection (adv_h; orange lines), vertical diffusion (Diff_v; blue lines), surface fluxes (surf; red lines), and shortwave fluxes (SW; broken red lines).

behind the initial onset of sea ice loss.

The off-shelf regions of W Ant also experience upper-ocean warming, beginning in 2015 and peaking between 2017 and 2020, followed by a period of cooling (Figure 3C). However, the mechanisms driving this warming differ notably from those in E Ant. In E Ant, vertical mixing plays an early and sustained role, whereas in W Ant, vertical mixing contributes to warming only during specific years (2018, 2021 and 2022). Further, in contrast to E Ant, shortwave fluxes in W Ant exhibit negative anomalies even during years of reduced sea ice cover, such as 2016, 2017, 2019 and 2020. Concurrently, the remaining surface flux components show positive anomalies. This pattern suggests warming due to reduced heat loss via longwave radiation in W Ant, in contrast to E Ant, where reduced sea ice consistently coincides with increased shortwave flux and negative anomalies in the other surface fluxes.

To examine the components of surface heat fluxes in greater detail, we analysed ERA5 heat flux fields over the off-shelf regions of E Ant and W Ant. The results reveal patterns consistent with those observed in SOSE (Figure 4). In E Ant, periods of enhanced SIE correspond to negative anomalies in shortwave fluxes. Conversely, during periods of reduced SIE, shortwave fluxes exhibit positive (warming) anomalies, while longwave fluxes display negative anomalies (Figure 4A).

In W Ant, however, reduced SIE does not always result in positive shortwave flux anomalies. In some years, such as 2016, 2017, 2019 and 2020, shortwave fluxes exhibit negative anomalies (cooling tendency), while longwave fluxes display positive anomalies (Figure 4C). This pattern is associated with enhanced cloud cover over the region (broken blue line; Figure 4C) and aligns with previous studies (*21, 32*) that associate intensified cloudiness with the poleward advection of warm, humid subtropical air driven by a strengthened ZW3 pattern.

A warming anomaly is also evident in the net surface fluxes in 2023 (Figure 4D), initiating renewed upper-ocean warming in W Ant (Figure 3D). In the earlier sea ice budget analysis, we noted a divergence between SOSE and observations in 2022 and 2023, with SOSE failing to capture the observed sea ice decline. However, the heat budget indicates that SOSE does simulate renewed upper-ocean warming during this period—suggesting that sea ice loss may eventually follow. This points to a possible lag in SOSE's sea ice response to oceanic warming, rather than a fundamental disagreement with observed trends.

In E Ant, reduced sea ice generally coincided with decreased cloud cover, allowing more shortwave input, and warming that was further enhanced by vertical mixing. In contrast, in W Ant, reduced sea ice often coincided with increased cloud cover, which limited shortwave

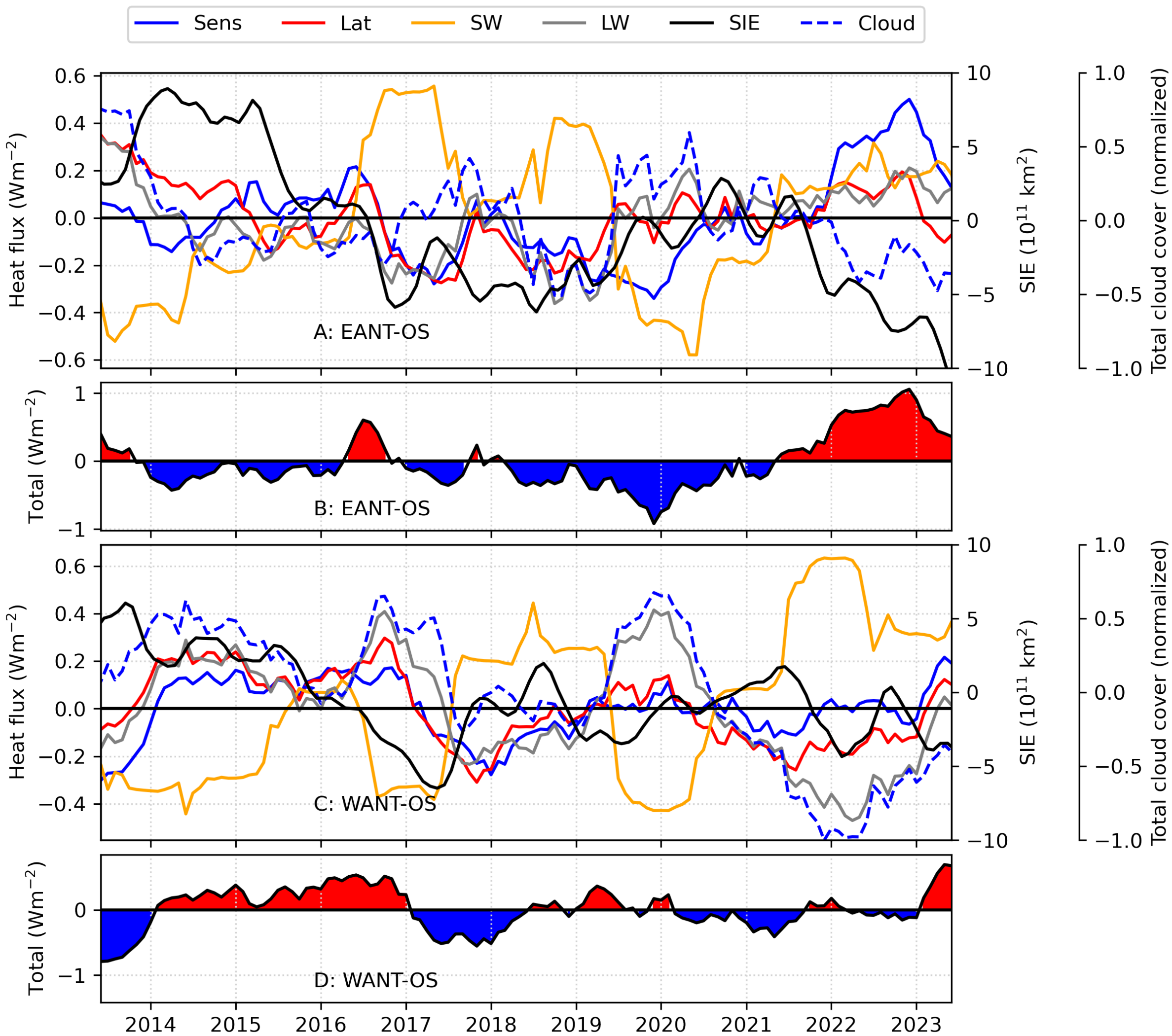

Figure 4: **Surface heat flux anomalies from ERA5** over the off-shelf regions of Antarctica. Panels **A** and **B** correspond to East Antarctica (E Ant), while **C** and **D** correspond to West Antarctica (W Ant). For each region, the first panel (**A** and **C**) shows anomalies in individual flux components—shortwave (SW; orange), latent (Lat; red), sensible (Sens; blue), and longwave (LW; gray)—along with sea ice extent anomaly (SIE; black, right-hand Y-axis) and total cloud cover anomaly (Cloud; broken blue, normalized). The second panel for each region (**B** and **D**) shows the net surface heat flux anomaly. All anomalies are relative to monthly climatologies, and for the purpose of visualization, time series are smoothed with a 12-month rolling mean to remove seasonal variability.

input but enhanced downward longwave radiation. This resulted in a distinct warming pathway, driven primarily by reduced longwave heat loss rather than increased shortwave absorption.

2.4 Upper-ocean salinity and stratification changes in the Southern Ocean

The upper ocean in E Ant displays a fresh anomaly from 2013 to 2015 (Figure S3). Thereafter, the upper ocean salinifies in E Ant (Figure 5A). Such salinification is accompanied by an increase in upper-ocean heat content. This is consistent with the hypothesis that the sea ice loss was driven by the upward mixing of heat and salt from within the CDW layer into the mixed layer, and points toward a prominent role of ocean dynamics in the sea ice decline.

W Ant, however, begins with an anomalously saline upper ocean, which progressively freshens from 2016 through 2023. As noted earlier, the loss in sea ice volume in this region is less pronounced than in E Ant, with off-shelf areas showing a recovery in sea ice volume after 2021. This is in accord with satellite-observed sea ice extent anomaly maps, which indicate positive SIE anomalies in parts of W Ant between 2016 and 2023 (Figure 9). The fresher upper ocean in W Ant is associated with positive anomalies in sea ice thickness during 2016, 2018, 2020, and from 2021 to 2023 (Supplementary Figure S2). This is consistent with the sea ice volume budget analysis, which showed a positive anomaly in the SIP term over the off-shelf W Ant during 2018-2021 (Figure 2H).

2.4.1 Salinity budgets off East Antarctica

We now examine spatially averaged salinities, and associated budget terms, to diagnose the causes of salinification over E Ant and of freshening over W Ant. E Ant upper-ocean salinification is associated with a decline in upper-ocean stratification ($\Delta\sigma$; defined as the difference between the potential density at depths of 240 m and 0 m), with a minimum in 2023 (Figures 5A and 5B). The increase in upper-ocean salinity is initially driven by the vertical advection term (grey line; Figures 5E and 5F), which exhibits a positive anomaly between 2013 and 2016. This term reflects the upwelling of salty waters and indicates a shoaling of the CDW layer, contributing to increased salinity in the uppermost 100 m. Vertical mixing also exhibits a positive anomaly in 2015 and 2016 (blue line; Figure 5E) over the off-shelf E Ant. Horizontal advection also contributed to salinification over the off-shelf E Ant during 2015-2016. Thus, both advective and diffusive terms contributed to the enhanced vertical and horizontal transfers of salt prior to 2016. We discuss the most likely driver of this salinification pathway in Section 2.5.

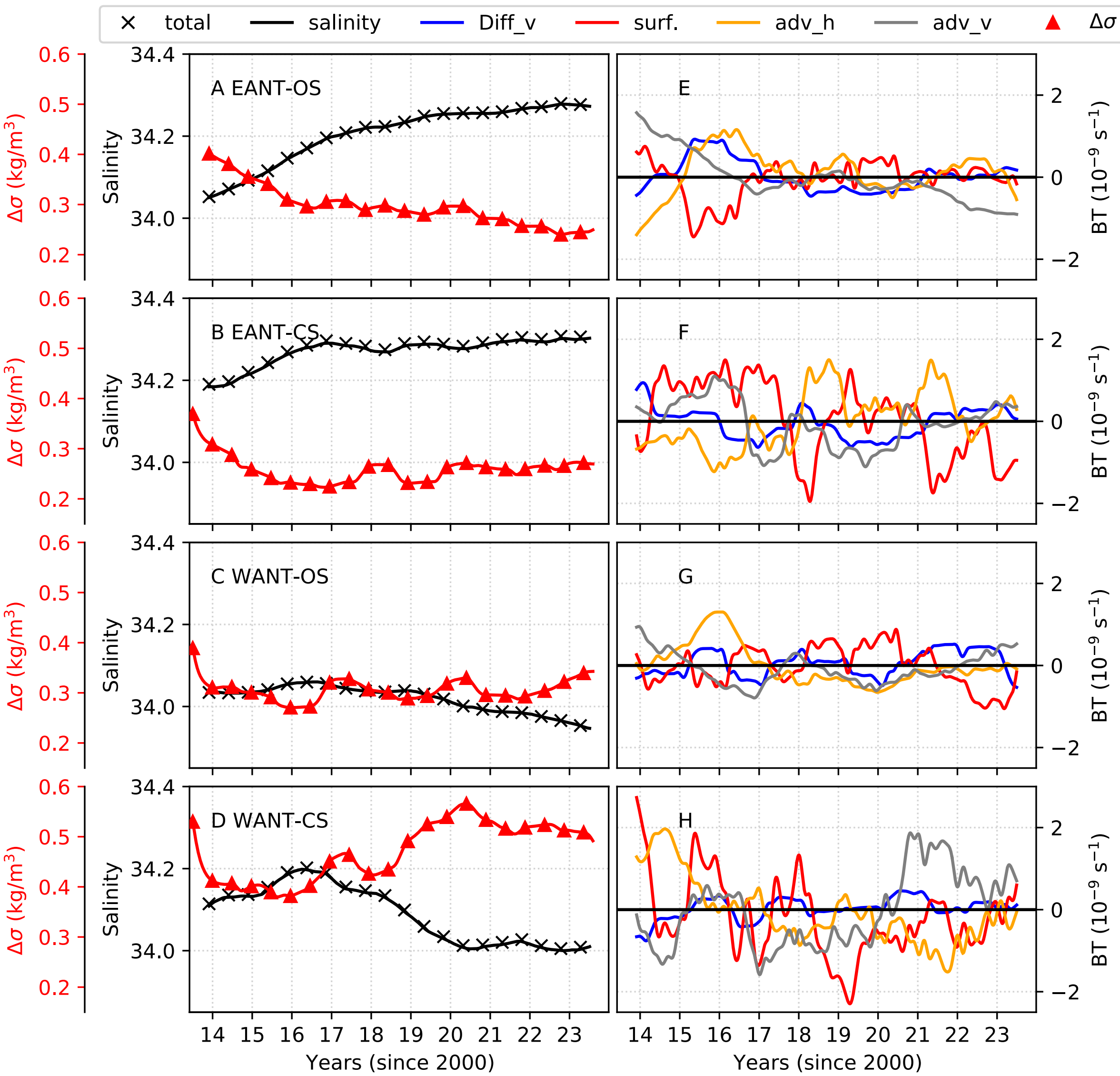

Figure 5: **SOSE salinity budget:** (**A-D.**) Salinity (black line with cross markers), vertically averaged over the upper 100 m, and spatially averaged over the regions labeled within the panels. A 12-month rolling mean was applied to remove the seasonality. The time-integrated sum of the budget terms is shown by cross markers. Also shown are the stratification (quantified by $\sigma^{\theta}_{240} - \sigma^{\theta}_{0}$; red line with triangle markers), spatially averaged in each region. (**E-H.**) Salinity budget terms are presented here as anomalies relative to their monthly means. Terms shown are the vertical advection (adv_v; grey lines), horizontal advection (adv_h; orange lines), vertical diffusion (Diff_v; blue lines), and surface fluxes (surf; red lines).

The surface flux term over the off-shelf E Ant showed a positive anomaly during 2013–2014, followed by a negative anomaly in 2015 and 2016. These patterns correspond to anomalies in SIP over the off-shelf E Ant (Figure 2F), indicating that the surface flux anomalies were induced by variations in sea ice formation. The positive anomalies in 2013–2014 reflect enhanced SIP, which increases salinity through brine rejection. In contrast, the negative anomalies in 2015 and 2016 coincide with reduced SIP, which led to upper-ocean freshening. This freshening resulted from both diminished brine rejection and increased export of sea ice from the continental shelf of E Ant, which melts during summer and deposits freshwater over the off-shelf regions.

2.4.2 Salinity budgets off West Antarctica

Salinity in the upper ocean over W Ant does not exhibit the increasing tendency seen over E Ant. Instead, salinity over the continental shelf of W Ant peaks in 2015 and 2016, and freshens thereafter, with an associated enhancement in stratification. The freshening and increased stratification are more pronounced over the continental shelf of W Ant, with the off-shelf W Ant experiencing a slight freshening in the years 2019-2023, with an associated enhancement of stratification.

W Ant freshening is explained by the persistent negative anomaly in the vertical advection term through the years 2015-2021 over the off-shelf W Ant (Figure 5G), and the years 2017-2019 over the continental shelf of W Ant (Figure 5H). Starting in 2020 and continuing through 2023, the vertical advection term shows signs of strengthening over both the continental shelf and off-shelf regions of W Ant.

The continental shelf of W Ant experienced a positive anomaly in the vertical advection term from 2020 to 2023, but this was balanced by a negative anomaly in the horizontal advection term. As a result, there is no change in upper-ocean salinity across these years except toward the end of 2023, when salinity increased and stratification decreased.

2.5 Surface stress forcing of salinity and stratification changes

To assess the drivers of the upper-ocean salinity and stratification changes shaping sea ice evolution, we revisit the vertical and horizontal advection terms of the salinity budget and compare them with surface stresses in SOSE. Surface stresses on the ocean reflect the combined effects of winds and sea ice drift. Vertical salinity advection is expected to respond to Ekman pumping driven by the cyclonicity of surface stresses, while meridional salinity advection in the upper

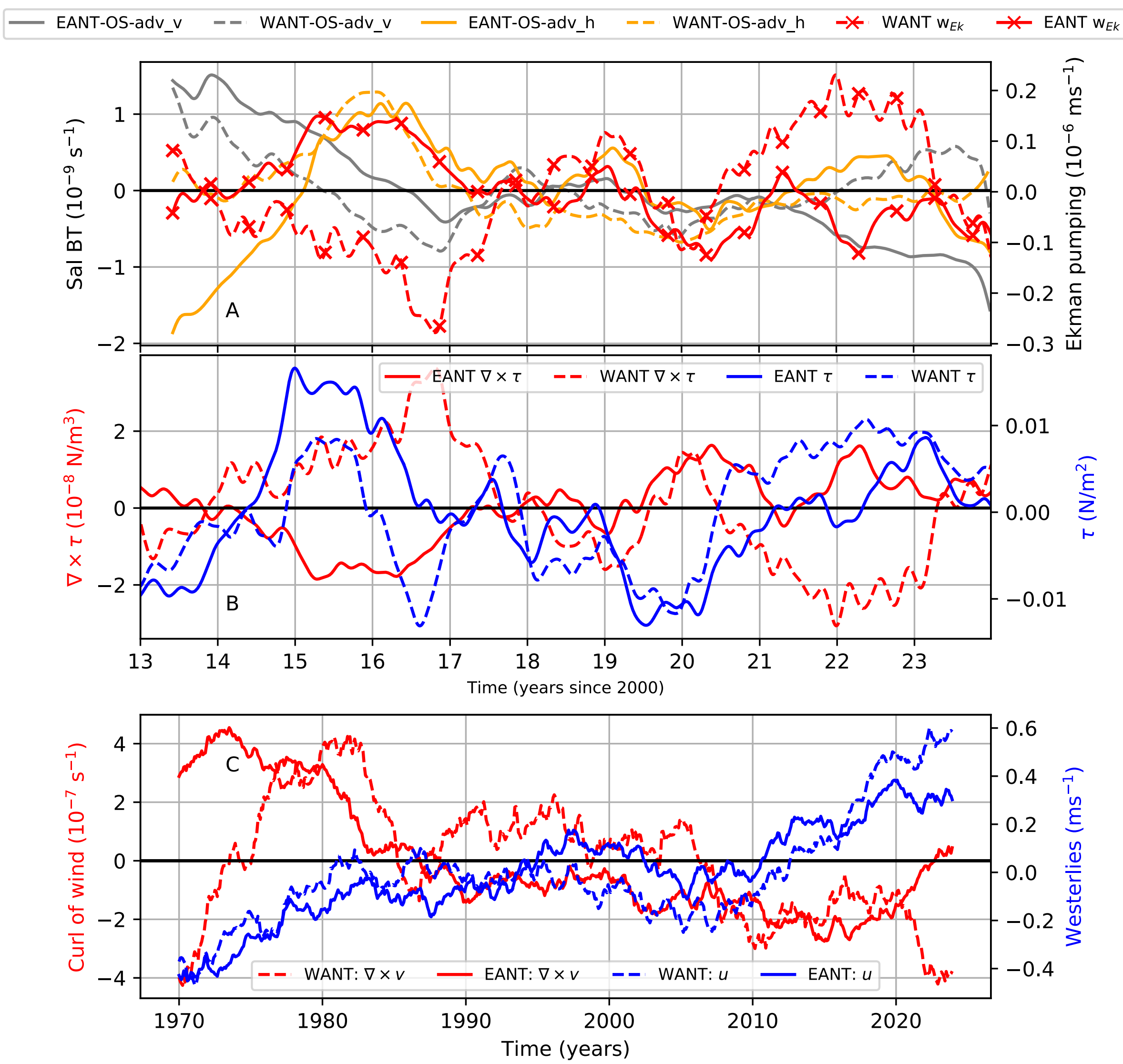

Figure 6: **Surface stresses and advection. A.** The vertical and horizontal salinity advection terms, and the Ekman pumping velocity (w_{Ek}), presented as anomalies (reproduced from Figure 5E-H) for off-shelf regions in E Ant and W Ant. **B.** Anomalies in the surface stress and stress curl over off-shelf regions in E Ant and W Ant. **C.** Anomalies in the curl of ERA5 wind velocity and in the ERA5 westerlies over the off-shelf regions of E Ant and W Ant. Time series in panels **A** and **B** are smoothed with a 12-month rolling mean to highlight interannual variability, while panel **C** uses a 10-year rolling mean to emphasize decadal trends.

ocean is anticipated to respond to zonal stresses. This analysis is restricted to the off-shelf regions of E Ant and W Ant. When computing the stress curl, the full (zonal and meridional) surface stress vector was considered, whereas anomalies in zonal stresses were computed using only positive (eastward) values. This approach is equivalent to using a spatial mask that selects the area with westerlies, which drive eastward stress and northward Ekman advection– a mechanism that has been proposed as a driver of sea ice loss (*17*).

As expected, during periods of enhanced cyclonicity in surface stress (negative anomalies in $\nabla \times \tau$, Figure 6B), the vertical salinity advection term exhibits anomalously positive values (grey lines in Figure 6A). Conversely, during periods of weakened cyclonicity in surface stress (positive anomalies in $\nabla \times \tau$, Figure 6B), the vertical advection term shows negative anomalies. SOSE reveals a zonal asymmetry in the stress curl: E Ant experiences intensified cyclonicity from 2013 to 2017, followed by a weakening; whereas W Ant exhibits weak cyclonicity from 2014 to 2017, which intensifies thereafter. This zonal asymmetry in the surface stress curl corresponds to a similar asymmetry in vertical advection across E Ant and W Ant.

A zonal asymmetry is also found in the eastward stress over E Ant and W Ant. Both regions exhibit an intensification between 2014 and 2016, and again from 2020 to 2023 (Figure 6B). However, the zonal stresses are generally stronger off E Ant between 2014 and 2016, whereas during 2020-2023 they are generally more intense off W Ant. The horizontal advection terms in E Ant and W Ant co-vary with the temporal variations of the eastward stress, suggesting that Ekman advection plays an important role in driving horizontal salinity advection anomalies in the upper ocean.

To contextualize these results within the multidecadal changes in Southern Ocean climate, we analyze ERA5 wind fields (monthly averages at 10 m above sea level) from 1970 to 2023 over the off-shelf regions of E Ant and W Ant (Figure 6C). Only the eastward component of the zonal wind is considered in computing "WANT: u" and "EANT: u". Wind curl and westerlies were computed as anomalies relative to their monthly means and smoothed using a 10-year rolling mean to capture interdecadal variability. The subpolar Southern Ocean has experienced a long-term intensification of wind curl over both E Ant and W Ant. Additionally, the westerlies have shown a sustained positive trend, reaching their highest magnitudes during the period from 2010 to 2023. The long-term trends in the winds indicate an intensification in the processes that induce upward transport of heat and salt from the subsurface ocean.

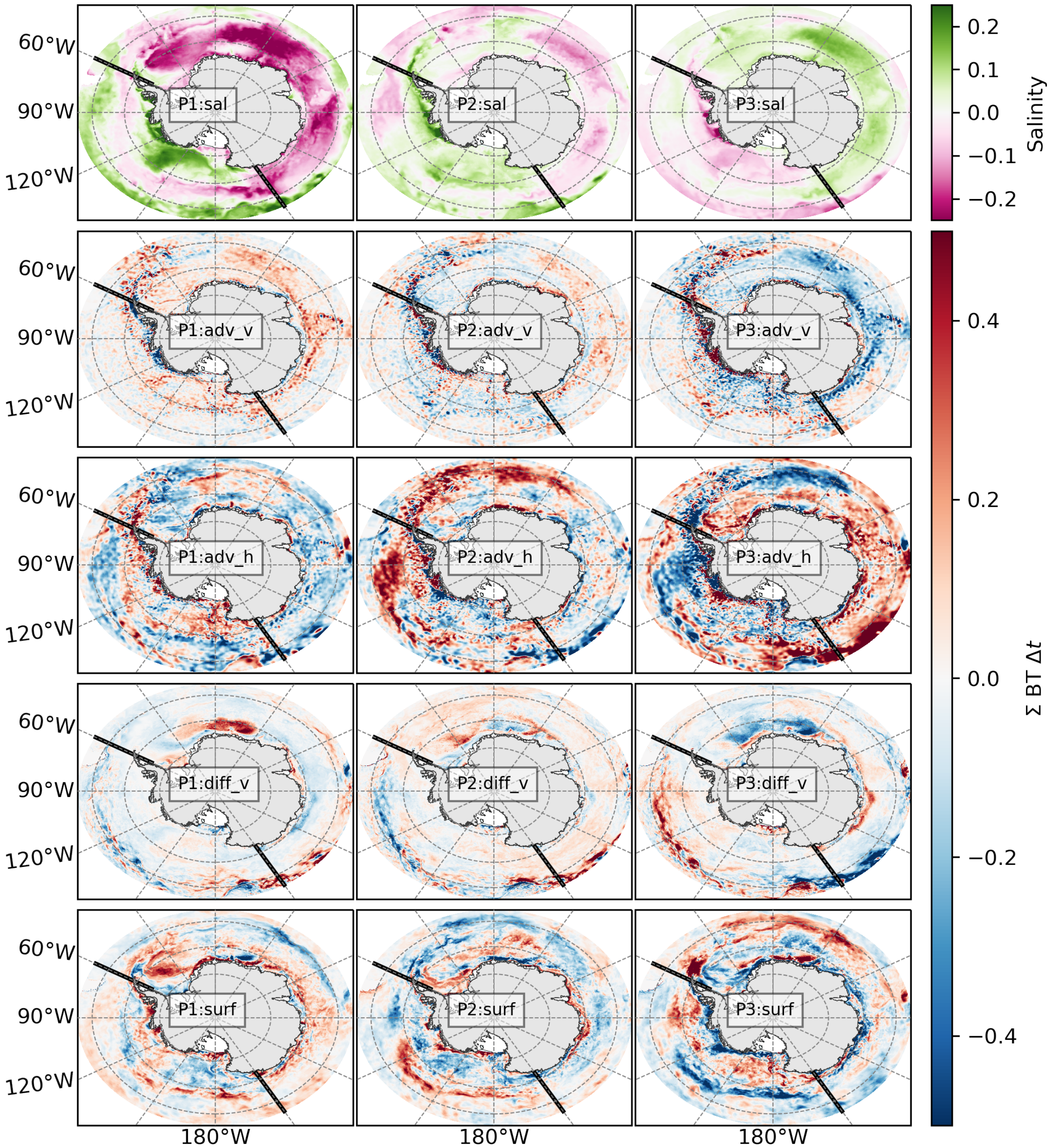

Figure 7: **Salinity budget maps**, time-integrated over periods: P1 (2013-06-01 through 2014), P2 (2015-2017), and P3 (2018-2023). Upper row shows salinity anomalies, and subsequent rows show the time-integrated salinity budget terms for vertical advection (adv_v), horizontal advection (adv_h), vertical diffusion (diff_v), and surface fluxes (surf). All terms are on the unit-less practical salinity scale (PSS (*52*)). Thick black lines mark the boundaries between E and W Ant at longitudes 150°E and 60°W.

2.6 Synthesis

The changes in Antarctic sea ice extent, and in upper-ocean hydrography and stratification, documented in the preceding sections may be synthesised into three distinct periods: P1 (mid 2013 to 2014), P2 (2015-2017), and P3 (2018-2023). These periods were selected based on the temporal evolution of sea ice volume in the off-shelf E Ant (Figure 2B), as this is the main contributor to total Antarctic sea ice volume changes. P1 corresponds to a period of elevated sea ice volume. P2 marks the onset of sea ice volume loss. And P3 captures the persistence of a low sea ice volume state with further decline.

During P1, the upper ocean exhibits a fresh anomaly across much of E Ant, while the W Ant region displays a saline anomaly (Figure 7; P1-sal to P3-sal). In P2, the magnitude of these anomalies diminishes overall. P3 is characterised by a salty anomaly in E Ant, and a fresh anomaly in W Ant. Saline and fresh anomalies are respectively associated with reduced and strengthened upper-ocean stratification.

During P1 (prior to 2015), the only budget term that displays a positive (salinifying) anomaly over the entire subpolar Southern Ocean is the vertical advection term (Figure 7; P1-adv_v). The surface flux term exhibits a positive anomaly everywhere except in the Ross Sea, off-shelf regions of the Amundsen and Bellingshausen seas, and the Eastern Weddell Sea. This is consistent with enhanced brine rejection due to stronger sea ice production in this period.

P2 (2015-2017) is characterised by sea ice loss, accompanied by an upper-ocean salinity increase across much of E Ant. The vertical advection term continues to salinify the upper ocean over large areas of E Ant, consistent with increased cyclonicity in the surface stress curl during this period. Generally, Ekman advection (which is a component of horizontal advection) moves cooler and fresher waters northward from high-latitude regions. Horizontal advection enhances salinity along the northern margins of the off-shelf regions, while exhibiting a freshening tendency in areas further south. This pattern occurs alongside positive anomalies in eastward surface stresses in E Ant, and a strong negative anomaly in surface stresses in W Ant during 2016. P2 is also characterised by increased vertical diffusion (Figure 7; P2-diff_v) across much of the subpolar Southern Ocean associated with intensified surface stresses that likely promote vertical mixing (see EANT-τ in Figure 6B). Surface fluxes show a freshening tendency near the sea ice margins, consistent with increased sea ice import from the continental shelf followed by melting offshore.

P3 exhibits a reversal of the zonal asymmetry in upper-ocean salinity, with salty anomalies in E Ant and fresh anomalies in W Ant (Figure 7; P3-sal). Vertical advection shows a freshening tendency, consistent with reduced cyclonicity in the surface stress curl over much of E Ant. In contrast, over the off-shelf W Ant, vertical advection exhibits a slight positive anomaly during this period. Salinification due to horizontal advection strengthens, aligning with enhanced surface stresses and increased northward Ekman advection of salt over much of E Ant. Surface fluxes indicate a salinifying tendency across the bulk of E Ant, consistent with decreased sea ice production in both the off-shelf and continental shelf regions. This leads to reduced sea ice (and freshwater) import into the off-shelf areas. In parts of the Ross and Amundsen seas in W Ant, however, surface fluxes freshen along the pack margins and salinify within the sea ice field, consistent with increased sea ice production on the continental shelves and reduced production and more melting in the off-shelf regions.

It is notable that our diagnosed mechanism during P3, wherein the surface fluxes act to salinify the upper ocean due to reduced sea ice export into the off-shelf E Ant regions, is the reverse of that reported by Haumann et al. (2016) during 1982-2008 (*11*). At that time, sea ice export was enhanced, leading to a freshening of the off-shelf regions. This reversal is in line with the oppositely-signed tendencies in sea ice extent in 1982-2008 vs. P3.

3 Discussion

We have shown that Antarctic sea ice loss in recent years was the compound result of a range of drivers acting in three distinct phases. This has led to a sustained low sea ice state unprecedented in the observational record (i.e. since the 1970s). These phases were most clearly observed in E Ant. At the start of the first phase (P1; 2013-2014), the upper ocean in E Ant was relatively cool and fresh. This was qualitatively consistent with the immediate response described by the two-timescale hypothesis (*40*), although we caution here that the hypothesis was based on idealized simulations that do not entirely capture the full complexity of the freshwater cycle that SOSE reveals. Further, P1 is also in accord with the Haumann et al. (2016) mechanism (*11*), wherein an expansion in sea ice extent caused freshening on the margins of E Ant. However, during P1-P2, vertical advection and mixing progressively increased the upper ocean's salinity, leading to a saltier state from P2 (2015-2017) through P3 (2018-2023) that qualitatively aligns with the longer-timescale response anticipated by the two-timescale hypothesis. Thus, the subsurface ocean played an important role in initiating upper-ocean warming and salinification that ultimately led to a pronounced sea ice loss in East Antarctica.

Additionally, we identify a third stage (P3) characterized by the response of surface fluxes to

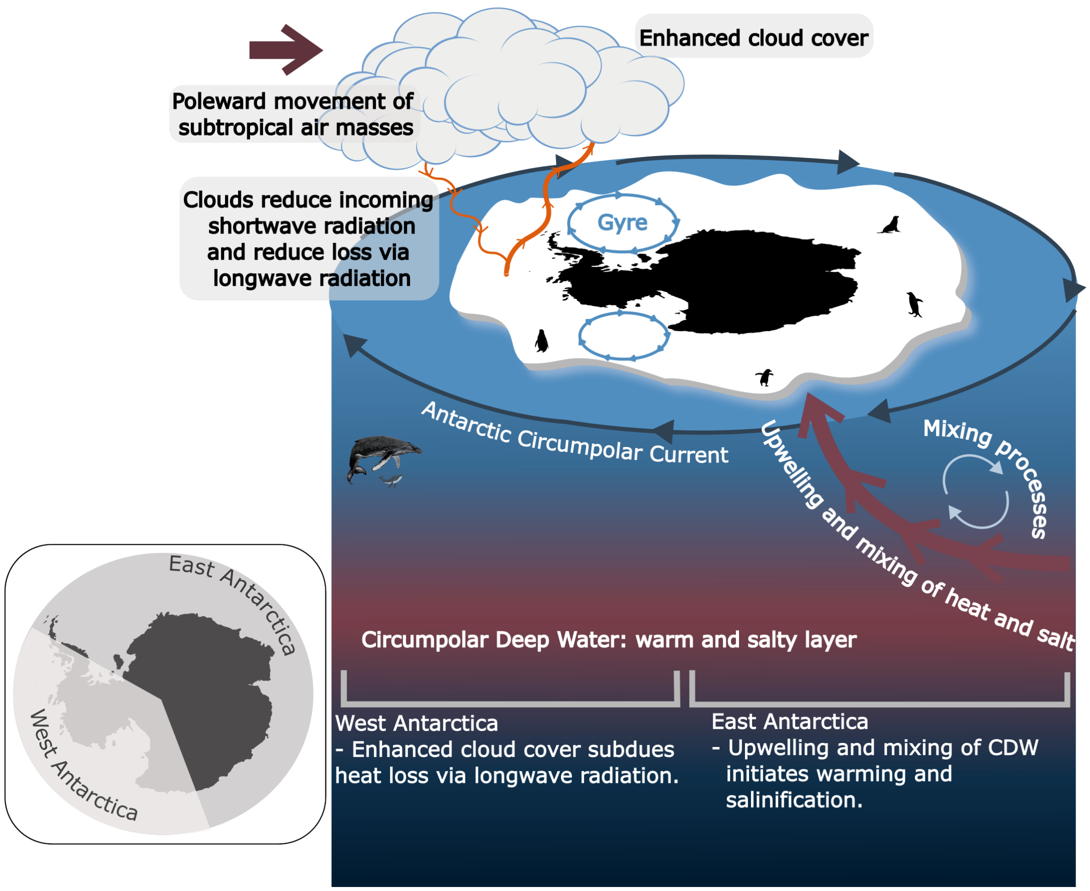

Figure 8: **Summary of processes** driving Antarctic sea ice loss. In West Antarctica, enhanced cloud cover associated with increased downward longwave radiation in years 2016, 2017, 2019, and 2020 drove sea ice loss. In East Antarctica, shoaling of the warm and salty Circumpolar Deep Water and the subsequent mixing of heat into the mixed layer during years 2013-2016 initiated sea ice loss.

sea ice loss. This response results in salinification of off-shelf regions due to a reduced import of freshwater via sea ice – a process analogous to a reversal of the Haumann et al. (2016) mechanism (*11*).

Sea ice loss in East Antarctica was initiated via heat input through the shoaling and mixing of heat from the CDW layer below the pycnocline. From 2015 to 2020, sea ice loss over the off-shelf regions resulted in increased sea ice production and freshwater export from the continental shelves. However, after 2020, sea ice production declined in both the off-shelf and continental shelf regions, leading to salinification due to reduced sea ice and freshwater import into the off-shelf areas of E Ant. These salty anomalies were redistributed by Ekman advection, forced by anomalous eastward surface stresses associated with intensified westerlies. Once sea ice was lost, the albedo feedback mechanism amplified heat gain through enhanced absorption of shortwave radiation. Doddridge et al. (2025) (*16*) used numerical experiments to show that this excess heat penetrates into the subsurface during summer and is re-entrained into the mixed layer during the subsequent winter, inhibiting sea ice growth.

Upper-ocean warming in E Ant was primarily initiated by the mixing of heat from below the pycnocline, whereas in W Ant, it was induced by enhanced downward longwave radiation associated with increased cloud cover. Schroeter et al. (2023) (*32*) demonstrated that the intensification of the ZW3 pattern enhanced the meridional transport of warm subtropical air masses toward the Ross, Amundsen and Bellingshausen seas from 2007 to 2021. Such meridional transport has been shown to impact sea ice via enhanced longwave radiative fluxes (*32, 53*). Further, Josey et al. (2024) (*12*) found that sea ice loss during 2023 was concentrated in regions of strong meridional transport, and was associated with enhanced ocean-to-atmosphere heat loss. A summary of processes identified in this study is provided in Figure 8.

The different balance of processes in E Ant vs. W Ant is manifested in a zonal asymmetry in upper-ocean salinification, which was driven by contrasting patterns of wind forcing between the two regions. W Ant begins with a saltier upper ocean, possibly due to enhanced Ekman pumping consistent with more intense wind curl over this region from 2009 to 2012 (Figure 6C). W Ant then gradually freshens after 2016, influenced by negative anomalies in the vertical advection term, which align with weaker surface stress curl over the region at that time. In contrast, E Ant experiences an enhancement in the cyclonicity of surface stresses, leading to increased Ekman pumping of salty warm waters toward the surface.

W Ant also experienced low sea ice conditions associated with upper-ocean saline anomalies. However, sea ice volume loss was less pronounced than in E Ant and showed a recovery in the off-shelf regions of W Ant after 2021. Observed sea ice extent also displayed a recovery in 2020 and 2021, but declined again thereafter. The W Ant upper ocean salinifies only weakly in 2022 and 2023, even though the vertical advection term supplies salt at a greater rate during this period (P3; 2018–2023; Figure 7). This salinification is driven by enhanced cyclonicity in the surface stress curl (Figure 6B). The slow response of upper-ocean salinity to this vertical advection may explain the apparent discrepancy in SOSE's sea ice extent during these years.

The SOSE run period captures the sea ice-ocean dynamics over the most recent decade, which encompasses the abrupt reduction in Antarctic sea ice of 2016. However, upwelling-favourable conditions occurred over a much longer period: a multidecadal trend toward enhanced cyclonicity in the winds over the subpolar Southern Ocean began in the 1980s (Figure 6C). Such intensification in wind cyclonicity coincided with a period of positive SAM that intensified the surface stresses (*24*). The Southern Ocean has also seen a multidecadal shoaling of the CDW layer and an accumulation of heat in the subsurface (*54–56*).

Enhanced wind stress and cyclonicity were found to precede anomalously low sea ice conditions in a model-based study (*41*). Reconstructions of past sea ice suggest a reduction in sea ice extent in the 1970s that took place under similar conditions of enhanced SAM and cyclonicity, with a greater loss seen over E Ant relative to W Ant (*57*).

Is the current decline in Antarctica sea ice a signal of a new regime in Southern Ocean dynamics, potentially locking the system into a persistent low sea ice state? Statistical analyses show evidence of a regime evolution in sea ice from 2007 onwards, finding increased variance and autocorrelation (*58*) and increased persistence in summer minima from year to year (*59*). Sea ice vorticity coupling with wind vorticity has increased, possibly indicating thinner sea ice overall (*60*). Predicting the future evolution of Southern Ocean sea ice requires caution, as climate models often struggle to accurately represent the complex processes governing the life-cycle of sea ice and its interplay with Southern Ocean dynamics, largely due to their coarse grid resolution and crude mixing parameterization schemes (*61*). Nevertheless, there is good reason to believe that upwelling-favourable conditions, driven by an enhanced SAM and intensified cyclonicity, are likely to persist under the influence of greenhouse gas emissions and the ozone hole (*27, 40*). These conditions are expected to facilitate upward mixing of CDW heat into the upper ocean, reinforcing the present low sea ice state.

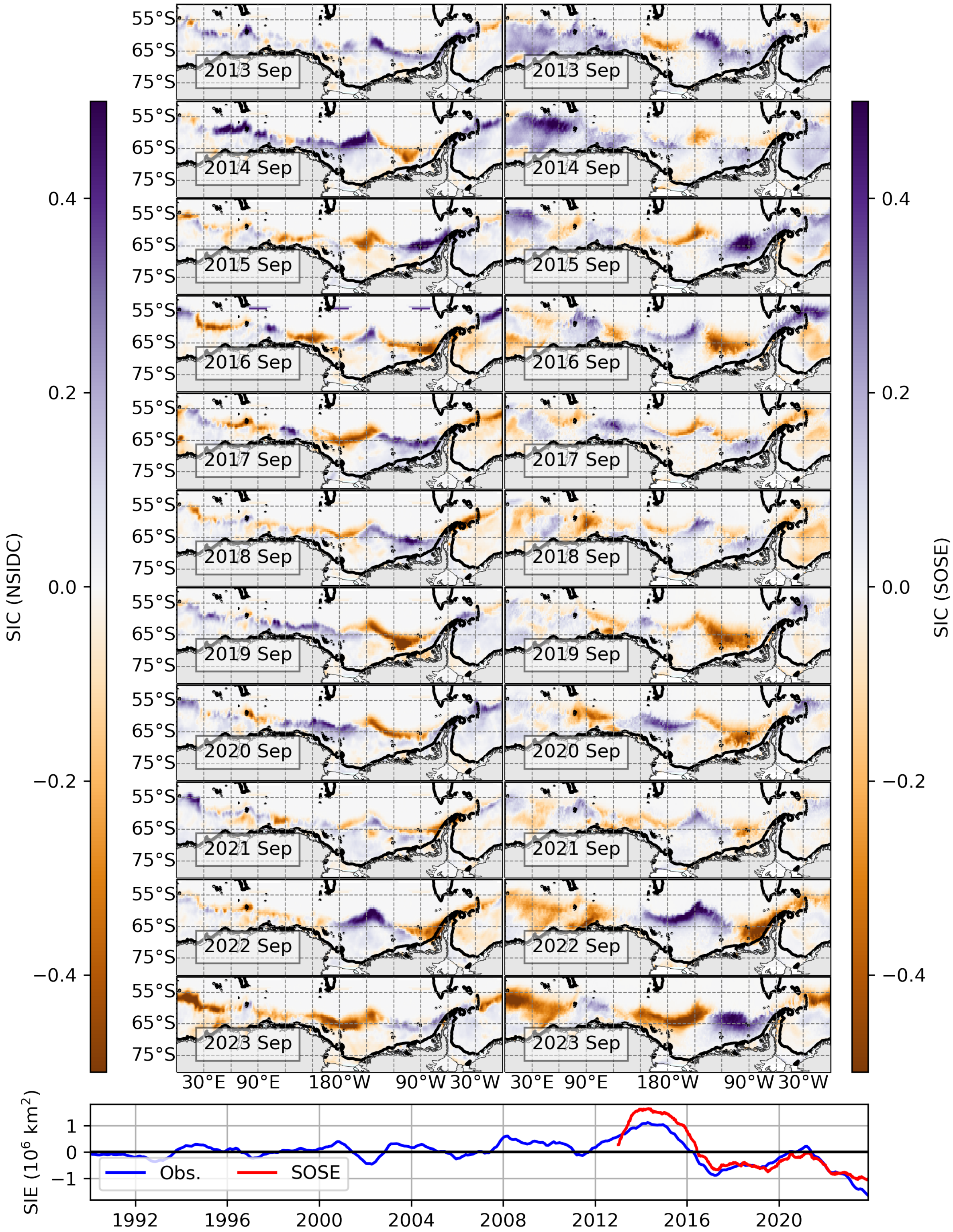

Figure 9: **Sea ice concentration anomaly** relative to the September mean (2013-2023) for satellite observations (left column) and for SOSE (right column). Lower panel shows the sea ice extent anomaly (SIE) in satellite observations (Obs.; blue line) and in SOSE (red line).

4 Methods

4.1 Southern Ocean State Estimate (SOSE)

The Biogeochemical Southern Ocean State Estimate (SOSE) is based on the MITgcm numerical ocean model with data assimilation through the adjoint method, which ensures that the assimilation scheme remains physically consistent (*62*). We used iteration-155 for this analysis (accessed from `https://sose.ucsd.edu/`), which has a horizontal resolution of 1/6º and 52 unevenly spaced vertical levels, and which runs from 2013 to 2023. The model iteratively assimilates *in situ* hydrographic profiles from Argo and tagged seals, and remotely sensed sea surface height, sea surface temperature and sea ice concentration. The assimilation does not introduce any unphysical nudging terms, and is carried out via the adjustment of the model's boundary forcing and initial conditions, hence preserving the budgets of conservative quantities. The atmospheric parameters were prescribed from ERA-5 fields at hourly intervals using boundary layer bulk formulae (*63*). The sea ice model represents the viscous-plastic rheology of ice and the thermodynamic equations governing its growth (*64*). Continental meltwater runoff is prescribed from the Hammond and Jones (2016) dataset (*65*), which is a multi-year average of freshwater fluxes from Antarctic ice shelves and ice sheets. This approach captures regional variation in meltwater discharge, but does not account for its temporal variability.

SOSE hydrography (*44*), sea ice properties (*66*), and thermodynamics (*3*) have been validated by numerous studies. Here, we extend the validation by comparing SOSE sea ice characteristics with satellite-based observations. Wintertime sea ice in SOSE is displaced equatorward compared to satellite data and shows a negative bias in the Weddell Sea, particularly pronounced between 0º and 60ºE (Figure S1). However, when examining the anomalies of each product relative to their own 11-year monthly-mean, the locations of positive and negative sea ice concentration anomalies are comparable between the two datasets (Figure 9). The sea ice extent (SIE) anomalies summed over the entire Southern Ocean are also comparable across the two datasets (lower panel; Figure 9). This provides confidence in our use of the state estimate to explore the mechanisms behind the observed sea ice loss.

We restrict this analysis to the model domain south of 50ºS. The model is fully equilibrated in terms of kinetic energy convergence, but the first six months of model output during 2013 are discarded, as the model hydrography and sea ice require time to evolve from the influence of the initial conditions. The analysis is spatially averaged over two regions: (1) West Antarctica (W Ant), defined between longitudes 150ºE and 300ºE, encompassing the Ross, Amundsen and

Bellingshausen Seas; and (2) East Antarctica (E Ant), which includes all regions outside of W Ant, covering the Weddell Sea and East Antarctica. Additionally, we define continental shelf (CS) regions as areas shallower than 3,000 m and south of 60ºS, with off-shelf (OS) regions comprising all areas beyond these criteria.

We consider the salinity (equivalent to salt concentration) budget:

$$\frac{\partial S}{\partial t} = G_{adv\_v} + G_{adv\_h} + G_{diff\_h} + G_{diff\_v} + G_{surf} \tag{1}$$

where the terms on the right hand side represent the salinity tendency due to vertical advection (G_{adv_v}), horizontal advection (G_{adv_h}), horizontal diffusion (G_{diff_h}), vertical diffusion (G_{diff_v}), and net surface fluxes (G_{surf}) due to evaporation, precipitation, meltwater runoff, and sea ice. All terms were stored online as 5-day averages. All salinity values are on the unit-less practical salinity scale (*52*), and the budget terms are in units of s^{-1}.

Similarly, a temperature (equivalent to heat) budget is evaluated:

$$\frac{\partial \theta}{\partial t} = G_{adv\_v} + G_{adv\_h} + G_{diff\_h} + G_{diff\_v} + G_{surf} \tag{2}$$

where the time tendency of potential temperature (θ in °C) is diagnosed as a function of vertical advection (G_{adv_v}), horizontal advection (G_{adv_h}), horizontal diffusion (G_{diff_h}), vertical diffusion (G_{diff_v}), and net surface fluxes (G_{surf}) of heat. The net surface fluxes integrate all surface heat flux components i.e. sensible, latent, longwave, and shortwave radiative fluxes. In this analysis, we separate out the shortwave component (SW) from the remaining surface components (surf). The budget terms are in units of $^{\circ}Cs^{-1}$. As for the salinity budget, all temperature budget terms were stored online as 5-day averages.

The sea ice volume (SIV) budget is computed as (*47*):

$$\frac{\partial \text{SIV}}{\partial t} = -\text{AD} + \text{SIP} \tag{3}$$

using the advection ($\mathbf{u_i} \cdot \nabla(\text{SIV})$) and divergence ($(\text{SIV})\,\nabla \mathbf{u_i}$) of sea ice, where $\mathbf{u_i}$ is the horizontal sea ice velocity. The residual was used to represent the *in situ* sea ice production (SIP). The sum of advection and divergence of sea ice volume (AD) represents the mechanical movement of sea ice, while sea ice production (SIP) represents the thermodynamic growth and melt of sea ice.

The Ekman pumping velocity is calculated using the total surface stress: $\text{w}_{Ek} = \frac{1}{\rho_0} \nabla \times (\frac{\tau}{f})$, where w_{Ek} is the vertical Ekman pumping velocity, the density of seawater $\rho_0 = 1,035$ kg m^{-3}, τ is the surface horizontal stress on the ocean from wind and sea ice, and $f = 2\Omega\, sin(\phi)$ is the Coriolis parameter, with the planetary angular velocity being $\Omega = 2\frac{\pi}{T}$, and the planet's rotational period as $T = 86\,400$ s.

4.2 Other methodological considerations

Satellite-observed sea ice concentration was obtained at daily frequency from the National Snow and Ice Data Center (*67*), and wind data was acquired as monthly averages from the ERA-5 reanalysis (*68*). Throughout this manuscript, all budget terms were smoothed using a 12-month rolling mean and a Butterworth filter with a window size of 90 days before being plotted. This was done to remove the seasonal signal, as the focus of this study is on interannual and longer-timescale variability. Numerical values represented as anomalies were computed within each spatial grid cell against the 11-year (2013-2023) monthly mean, after which they were spatially averaged.

References

1. A. Riihelä, R. M. Bright, K. Anttila. Recent strengthening of snow and ice albedo feedback driven by Antarctic sea-ice loss. *Nature Geoscience* **14**, 832–836 (2021).

2. V. Pellichero, J.-B. Sallée, C. C. Chapman, S. M. Downes. The Southern Ocean meridional overturning in the sea-ice sector is driven by freshwater fluxes. *Nature Communications* **9**, 1789 (2018).

3. R. P. Abernathey, I. Cerovecki, P. R. Holland, E. Newsom, M. Mazloff, L. D. Talley. Water-mass transformation by sea ice in the upper branch of the Southern Ocean overturning. *Nature Geoscience* **9**, 596 (2016).

4. L. Li, Z. Liu, C. Zhu, C. He, B. Otto-Bliesner. Shallowing glacial Antarctic Intermediate Water by changes in sea ice and hydrological cycle. *Geophysical Research Letters* **48**, e2021GL094317 (2021).

5. F. A. Haumann, N. Gruber, M. Münnich. Sea-ice induced southern ocean subsurface warming and surface cooling in a warming climate. *AGU Advances* **1**, e2019AV000132 (2020).

6. W. O. Smith Jr., J. C. Comiso. Influence of sea ice on primary production in the Southern Ocean: A satellite perspective. *Journal of Geophysical Research: Oceans* **113** (2008).

7. W. R. Hobbs, R. Massom, S. Stammerjohn, P. Reid, G. Williams, W. Meier. A review of recent changes in southern ocean sea ice, their drivers and forcings. *Global and Planetary Change* **143**, 228–250 (2016).

8. G. A. Meehl, J. M. Arblaster, C. M. Bitz, C. T. Y. Chung, H. Teng. Antarctic sea-ice expansion between 2000 and 2014 driven by tropical Pacific decadal climate variability. *Nature Geoscience* **9**, 590–595 (2016).

9. R. Bintanja, G. J. van Oldenborgh, S. S. Drijfhout, B. Wouters, C. A. Katsman. Important role for ocean warming and increased ice-shelf melt in Antarctic sea-ice expansion. *Nature Geoscience* **6**, 376–379 (2013).

10. P. R. Holland, R. Kwok. Wind-driven trends in antarctic sea-ice drift. *Nature Geoscience* **5**, 872 (2012).

11. F. A. Haumann, N. Gruber, M. Münnich, I. Frenger, S. Kern. Sea-ice transport driving Southern Ocean salinity and its recent trends. *Nature* **537**, 89–92 (2016).

12. S. A. Josey, A. J. S. Meijers, A. T. Blaker, J. P. Grist, J. Mecking, H. C. Ayres. Record-low Antarctic sea ice in 2023 increased ocean heat loss and storms. *Nature* **636**, 635–639 (2024).

13. A. Purich, E. W. Doddridge. Record low antarctic sea ice coverage indicates a new sea ice state. *Communications Earth & Environment* **4**, 1–9 (2023).

14. A. Silvano, A. Narayanan, R. Catany, E. Olmedo, V. González-Gambau, A. Turiel, R. Sabia, M. R. Mazloff, T. Spira, F. A. Haumann, A. C. Naveira Garabato. Rising surface salinity and declining sea ice: A new southern ocean state revealed by satellites. *Proceedings of the National Academy of Sciences* **122**, e2500440122 (2025).

15. R. Ferrari, M. F. Jansen, J. F. Adkins, A. Burke, A. L. Stewart, A. F. Thompson. Antarctic sea ice control on ocean circulation in present and glacial climates. *Proceedings of the National Academy of Sciences* **111**, 8753–8758 (2014).

16. E. W. Doddridge, *et al.*. Impacts of antarctic summer sea-ice extremes. *PNAS Nexus* **4**, pgaf164 (2025).

17. E. A. Wilson, D. B. Bonan, A. F. Thompson, N. Armstrong, S. C. Riser. Mechanisms for abrupt summertime circumpolar surface warming in the Southern Ocean. *Journal of Climate* **36**, 7025–7039 (2023).

18. D. Francis, C. Eayrs, J. Cuesta, D. Holland. Polar Cyclones at the Origin of the Reoccurrence of the Maud Rise Polynya in Austral Winter 2017. *Journal of Geophysical Research: Atmospheres* **124**, 5251 (2019).

19. E. C. Campbell, E. A. Wilson, G. W. K. Moore, S. C. Riser, C. E. Brayton, M. R. Mazloff, L. D. Talley. Antarctic offshore polynyas linked to Southern Hemisphere climate anomalies. *Nature* **570**, 319 (2019).

20. B. Jena, C. C. Bajish, J. Turner, M. Ravichandran, N. Anilkumar, S. Kshitija. Record low sea ice extent in the Weddell Sea, Antarctica in april/may 2019 driven by intense and explosive polar cyclones. *npj Climate and Atmospheric Science* **5**, 1–15 (2022).

21. M. N. Raphael. The influence of atmospheric zonal wave three on Antarctic sea ice variability. *Journal of Geophysical Research: Atmospheres* **112** (2007).

22. E. Schlosser, F. A. Haumann, M. N. Raphael. Atmospheric influences on the anomalous 2016 Antarctic sea ice decay. *The Cryosphere* **12**, 1103–1119 (2018).

23. J. Turner, T. Phillips, G. J. Marshall, J. S. Hosking, J. O. Pope, T. J. Bracegirdle, P. Deb. Unprecedented springtime retreat of antarctic sea ice in 2016. *Geophysical Research Letters* **44**, 6868–6875 (2017).

24. G. A. Meehl, J. M. Arblaster, C. T. Y. Chung, M. M. Holland, A. DuVivier, L. Thompson, D. Yang, C. M. Bitz. Sustained ocean changes contributed to sudden Antarctic sea ice retreat in late 2016. *Nature Communications* **10**, 14 (2019).

25. G. Wang, H. H. Hendon, J. M. Arblaster, E.-P. Lim, S. Abhik, P. van Rensch. Compounding tropical and stratospheric forcing of the record low Antarctic sea-ice in 2016. *Nature Communications* **10**, 13 (2019).

26. A. Purich, M. H. England. Tropical teleconnections to Antarctic sea ice during austral spring 2016 in coupled pacemaker experiments. *Geophysical Research Letters* **46**, 6848–6858 (2019).

27. R. L. Fogt, G. J. Marshall. The Southern Annular Mode: Variability, trends, and climate impacts across the Southern Hemisphere. *WIREs Climate Change* **11**, e652 (2020).

28. J. Marshall, K. C. Armour, J. R. Scott, Y. Kostov, U. Hausmann, D. Ferreira, T. G. Shepherd, C. M. Bitz. The ocean's role in polar climate change: asymmetric Arctic and Antarctic responses to greenhouse gas and ozone forcing. *Philosophical Transactions of the Royal Society A: Mathematical, Physical and Engineering Sciences* **372**, 20130040 (2014).

29. W. G. Cheon, A. L. Gordon. Open-ocean polynyas and deep convection in the Southern Ocean. *Scientific Reports* **9**, 6935 (2019).

30. S. K. Lee, R. Lumpkin, F. Gomez, S. Yeager, H. Lopez, F. Takglis, S. Dong, W. Aguiar, D. Kim, M. Baringer. Human-induced changes in the global meridional overturning circulation are emerging from the southern ocean. *Communications Earth & Environment* **4**, 1 (2023).

31. L. Olivier, F. A. Haumann. Southern ocean freshening stalls deep ocean co2 release in a changing climate (2025).

32. S. Schroeter, T. J. O'Kane, P. A. Sandery. Antarctic sea ice regime shift associated with decreasing zonal symmetry in the southern annular mode. *The Cryosphere* **17**, 701–717 (2023).

33. M. D. Eabry, R. Goyal, A. S. Taschetto, W. Hobbs, A. S. Gupta. Combined impacts of southern annular mode and zonal wave 3 on antarctic sea ice variability. *Journal of Climate* **37**, 1759–1775 (2024).

34. N. C. Swart, S. T. Gille, J. C. Fyfe, N. P. Gillett. Recent southern ocean warming and freshening driven by greenhouse gas emissions and ozone depletion. *Nature Geoscience* **11**, 836–841 (2018).

35. T. J. Bracegirdle, G. Krinner, M. Tonelli, F. A. Haumann, K. A. Naughten, T. Rackow, L. A. Roach, I. Wainer. Twenty first century changes in Antarctic and Southern Ocean surface climate in CMIP6. *Atmospheric Science Letters* **21**, e984 (2020).

36. Q. Li, M. H. England, A. M. Hogg, S. R. Rintoul, A. K. Morrison. Abyssal ocean overturning slowdown and warming driven by antarctic meltwater. *Nature* **615**, 841–847 (2023).

37. C. de Lavergne, J. B. Palter, E. D. Galbraith, R. Bernardello, I. Marinov. Cessation of deep convection in the open Southern Ocean under anthropogenic climate change. *Nature Clim. Change* **4**, 278 (2014).

38. Q. Li, M. H. England, A. M. C. Hogg, S. R. Rintoul, A. K. Morrison. Abyssal ocean overturning slowdown and warming driven by antarctic meltwater. *Nature* **615**, 841 (2023).

39. T. Spira, M. D. Plessis, F. A. Haumann, A. Narayanan, A. Silvano, S. Swart, I. Giddy. Wind-triggered antarctic sea ice decline preconditioned by thinning winter water (2025).

40. D. Ferreira, J. Marshall, C. M. Bitz, S. Solomon, A. Plumb. Antarctic ocean and sea ice response to ozone depletion: A two-time-scale problem. *Journal of Climate* **28**, 1206–1226 (2015).

41. Y. Morioka, S. Manabe, L. Zhang, T. L. Delworth, W. Cooke, M. Nonaka, S. K. Behera. Antarctic sea ice multidecadal variability triggered by southern annular mode and deep convection. *Communications Earth & Environment* **5**, 1–11 (2024).

42. L. Zhang, T. L. Delworth, X. Yang, F. Zeng, F. Lu, Y. Morioka, M. Bushuk. The relative role of the subsurface Southern Ocean in driving negative Antarctic sea ice extent anomalies in 2016–2021. *Communications Earth & Environment* **3**, 1–9 (2022).

43. L. A. Roach, J. Dörr, C. R. Holmes, F. Massonnet, E. W. Blockley, D. Notz, T. Rackow, M. N. Raphael, S. P. O'Farrell, D. A. Bailey, *et al.*. Antarctic sea ice area in CMIP6. *Geophysical Research Letters* **47**, e2019GL086729 (2020).

44. A. Verdy, M. R. Mazloff. A data assimilating model for estimating southern ocean biogeochemistry. *Journal of Geophysical Research: Oceans* **122**, 6968–6988 (2017).

45. A. Narayanan, S. T. Gille, M. R. Mazloff, M. D. du Plessis, K. Murali, F. Roquet. Zonal distribution of Circumpolar Deep Water transformation rates and its relation to heat content on Antarctic shelves. *Journal of Geophysical Research: Oceans* **128**, e2022JC019310 (2023).

46. H. Chen, F. A. Haumann, L. D. Talley, K. S. Johnson, J. L. Sarmiento. The deep ocean's carbon exhaust. *Global Biogeochemical Cycles* **36**, e2021GB007156 (2022).

47. K. Himmich, M. Vancoppenolle, S. Stammerjohn, M. Bocquet, G. Madec, J.-B. Sallée, S. Fleury. Thermodynamics drive post-2016 changes in the Antarctic sea ice seasonal cycle. *Journal of Geophysical Research: Oceans* **129**, e2024JC021112 (2024).

48. D. Stappard, B. Fernández Castro, A. Naveira Garabato, T. Tyrrell. Identification of southern ocean upwelling from biogeochemical-argo floats. *Journal of Geophysical Research: Oceans* **130**, e2023JC020597 (2025).

49. D. G. Martinson. Evolution of the Southern Ocean winter mixed layer and sea ice: Open ocean deepwater formation and ventilation. *Journal of Geophysical Research: Oceans* **95**, 11641 (1990).

50. E. A. Wilson, S. C. Riser, E. C. Campbell, A. P. S. Wong. Winter upper-ocean stability and ice–ocean feedbacks in the sea ice–covered Southern Ocean. *Journal of Physical Oceanography* **49**, 1099–1117 (2019).

51. F. Roquet, D. Ferreira, R. Caneill, D. Schlesinger, G. Madec. Unique thermal expansion properties of water key to the formation of sea ice on Earth. *Science Advances* **8**, eabq0793 (2022).

52. E. L. Lewis, R. Perkin. Salinity: Its definition and calculation. *Journal of Geophysical Research: Oceans* **83**, 466 (1978).

53. D. Francis, K. S. Mattingly, M. Temimi, R. Massom, P. Heil. On the crucial role of atmospheric rivers in the two major Weddell Polynya events in 1973 and 2017 in Antarctica. *Science Advances* **6**, eabc2695 (2020). Publisher: American Association for the Advancement of Science.

54. S. Schmidtko, K. J. Heywood, A. F. Thompson, S. Aoki. Multidecadal warming of Antarctic waters. *Science* **346**, 1227 (2014).

55. S. T. Gille. Warming of the Southern Ocean since the 1950s. *Science* **295**, 1275–1277 (2002).

56. L. Herraiz-Borreguero, A. C. Naveira Garabato. Poleward shift of circumpolar deep water threatens the east antarctic ice sheet. *Nature Climate Change* **12**, 728–734 (2022).

57. H. Goosse, Q. Dalaiden, F. Feba, B. Mezzina, R. L. Fogt. A drop in antarctic sea ice extent at the end of the 1970s. *Communications Earth & Environment* **5**, 1–11 (2024).

58. W. Hobbs, P. Spence, A. Meyer, S. Schroeter, A. D. Fraser, P. Reid, T. R. Tian, Z. Wang, G. Liniger, E. W. Doddridge, P. W. Boyd. Observational evidence for a regime shift in summer antarctic sea ice. *Journal of Climate* **37**, 2263–2275 (2024).

59. M. N. Raphael, T. J. Maierhofer, R. L. Fogt, W. R. Hobbs, M. S. Handcock. A twenty-first century structural change in antarctica's sea ice system. *Communications Earth & Environment* **6**, 1–9 (2025).

60. W. de Jager, M. Vichi. Increased rotational coupling between antarctic sea ice and the atmosphere over the last 30 years. *Journal of Geophysical Research: Oceans* **130**, e2024JC021239 (2025).

61. M. Mohrmann, C. Heuzé, S. Swart. Southern ocean polynyas in cmip6 models. *The Cryosphere* **15**, 4281–4313 (2021).

62. M. R. Mazloff, P. Heimbach, C. Wunsch. An eddy-permitting Southern Ocean state estimate. *Journal of Physical Oceanography* **40**, 880 (2010).

63. W. G. Large, S. G. Yeager, Diurnal to decadal global forcing for ocean and sea-ice models: The data sets and flux climatologies (2004).

64. M. Losch, D. Menemenlis, J.-M. Campin, P. Heimbach, C. Hill. On the formulation of sea-ice models. Part 1: Effects of different solver implementations and parameterizations. *Ocean Modelling* **33**, 129–144 (2010).

65. M. D. Hammond, D. C. Jones. Freshwater flux from ice sheet melting and iceberg calving in the Southern Ocean. *Geoscience Data Journal* **3**, 60 (2016).

66. A. Narayanan, F. Roquet, S. T. Gille, B. Gülk, M. R. Mazloff, A. Silvano, A. C. Naveira Garabato. Ekman-driven salt transport as a key mechanism for open-ocean polynya formation at maud rise. *Science Advances* **10**, eadj0777 (2024).

67. W. N. Meier, J. S. Stewart, H. Wilcox, M. A. Hardman, D. J. Scott., Near-real-time DMSP SSMIS daily polar gridded sea ice concentrations, Version 2.0081, https://nsidc.org/data/nsidc-0081 (2021).

68. ERA5, ERA5: Fifth generation of ECMWF atmospheric reanalyses of the global climate . Copernicus Climate Change Service Climate Data Store (CDS) (2019). Accessed on July 2019 from https://cds.climate.copernicus.eu/cdsapp#!/home.

Acknowledgments

Funding

AN and ACNG acknowledge funding from the NERC DeCAdeS project (NE/T012714/1). MRM acknowledges funding from NSF grants OPP-2332379, OPP-2149501, OCE-1924388, and OPP-2319829, and NASA grants 80NSSC22K0387, 80NSSC20K1076, and 80NSSC24K0243. MHE acknowledges funding from ARC Grants SR200100008 and DP190100494. FAH is supported by the European Union (ERC, VERTEXSO, 101041743) and the Initiative and Networking Fund of the Helmholtz Association (VH-NG-19-33). ACNG acknowledges UKRI guarantee funding for an ERC Advanced Grant (EP/X025136/1). HA acknowledges funding from the NERC DIMSUM project (NE/Y005090/1). SZ acknowledge funding from the OCEAN ICE project, which is co-funded by the European Union Horizon Europe Funding Programme for research and innovation under grant agreement Nr. 101060452 and by UK Research and Innovation.

Author Contributions

Conceptualization: AN, AS, ACNG
Methodology: AN, AS, ACNG, MRM
Investigation: AN, HA, AS, ACNG, MRM, TS, FAH, MHE, SZ
Visualization: AN
Supervision: AS, ACNG
Writing original draft: AN, HA, AS, ACNG, TS, FAH, MHE, SZ
Writing – review and editing: AN, HA, AS, ACNG, MRM, TS, FAH, MHE, SZ

Competing interests

The authors declare that they have no competing interests.

Data and materials availability

All data needed to evaluate the conclusions in the paper are present in the paper and/or the Supplementary Materials. All SOSE data used in this study are available at `http://sose.ucsd.edu/`. All software code used to produce this analysis are available at: `https://osf.io/k87dw/?view_only=bd444f2076734efa8ff310b4b1fd0628`. All observations are available as open-access datasets through the DOI links provided in their references.

Supplementary Material for: “Compound Drivers of Antarctic Sea Ice Loss”

Aditya Narayanan, School of Ocean and Earth Sciences
University of Southampton,
National Oceanography Centre Southampton, UK (a.narayanan@soton.ac.uk)

Contents of this file

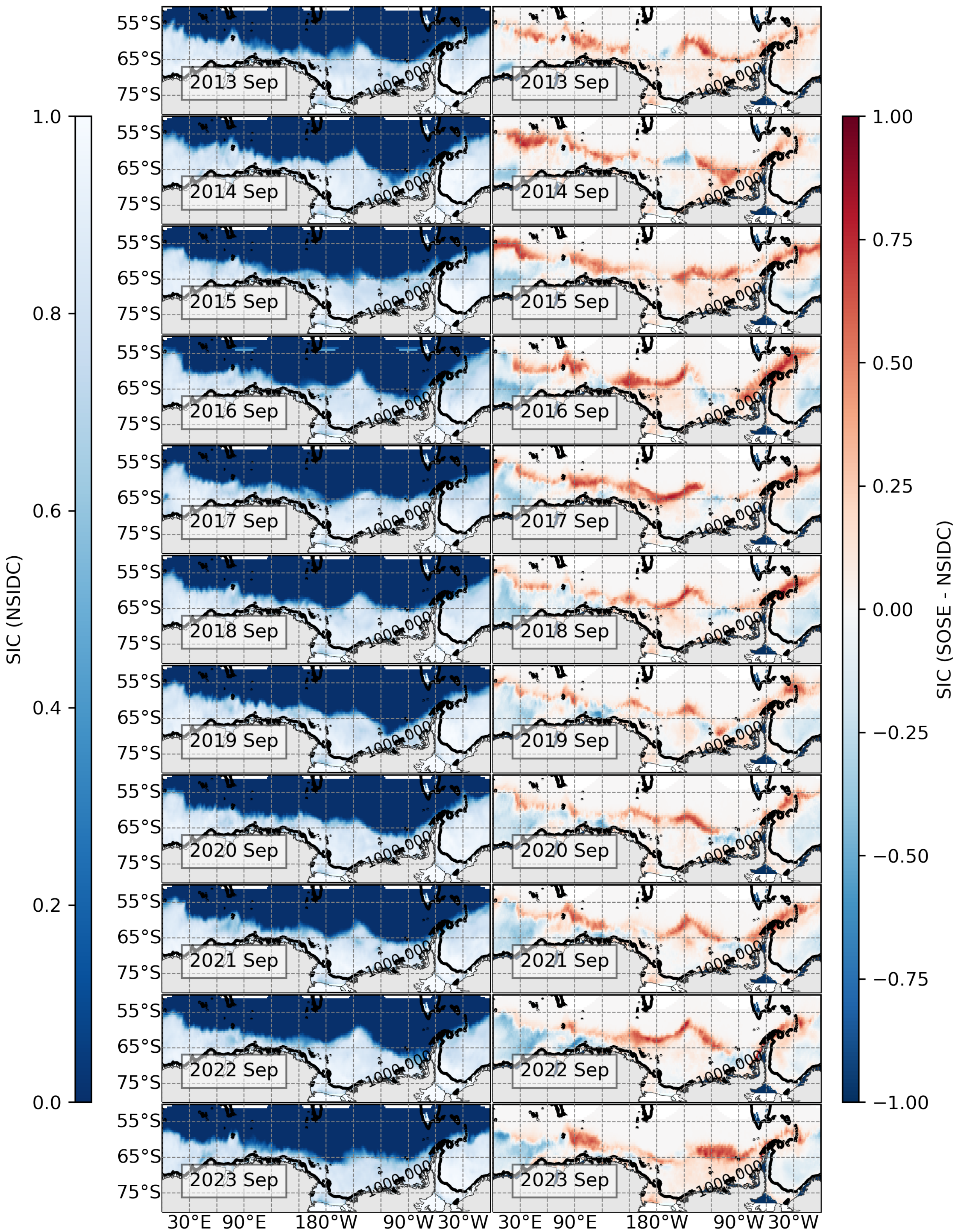

Figure S1: Sea ice concentrations (SIC) observed by satellites, averaged in September, is shown on the left hand column. SOSE SIC minus satellite-observed SIC, averaged in September, is shown on the right hand column.

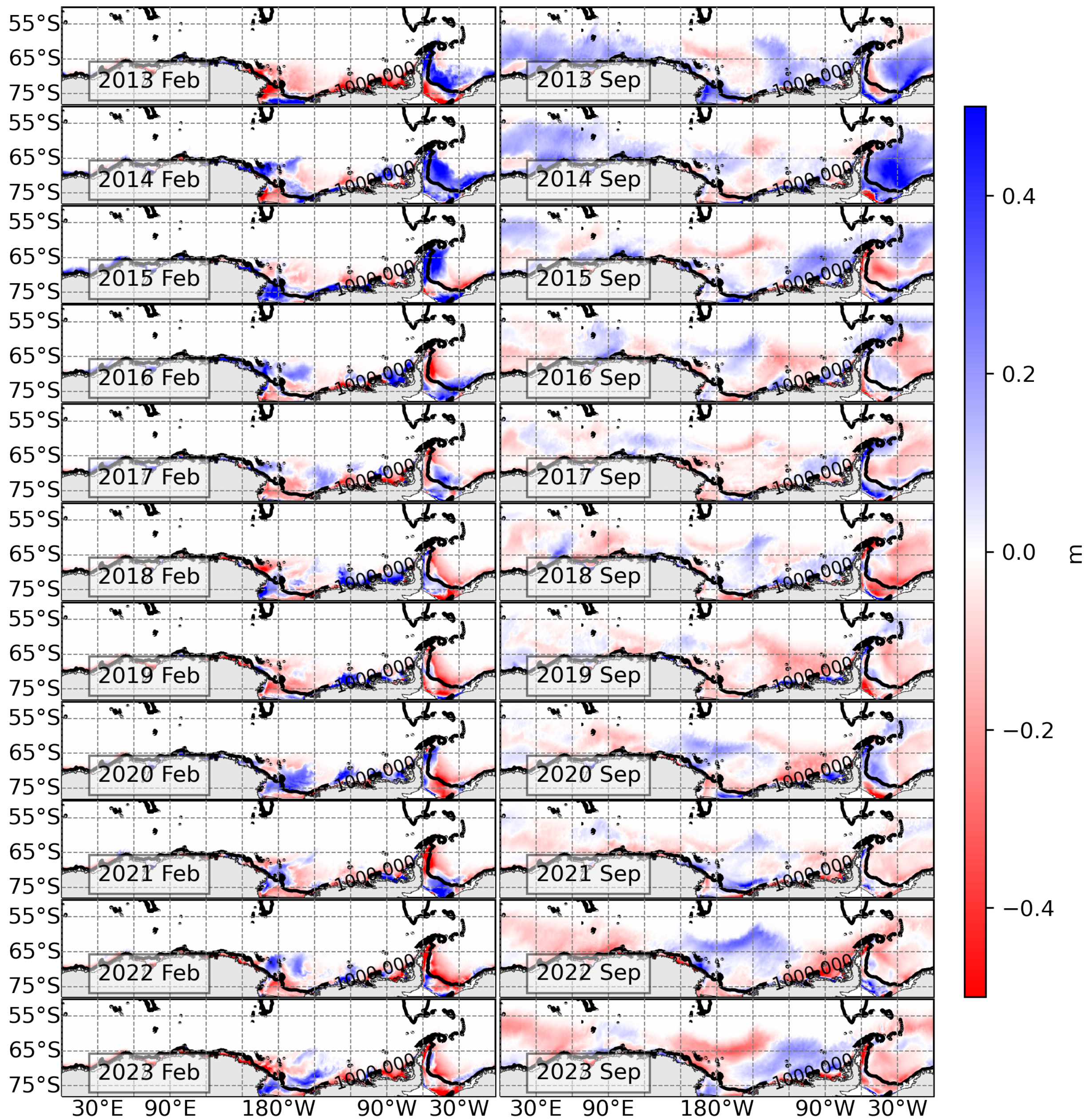

Figure S2: Sea ice thickness from SOSE represented as anomalies with respect to the 11-year monthly means, shown here for February (left hand column) and for September (right hand column).

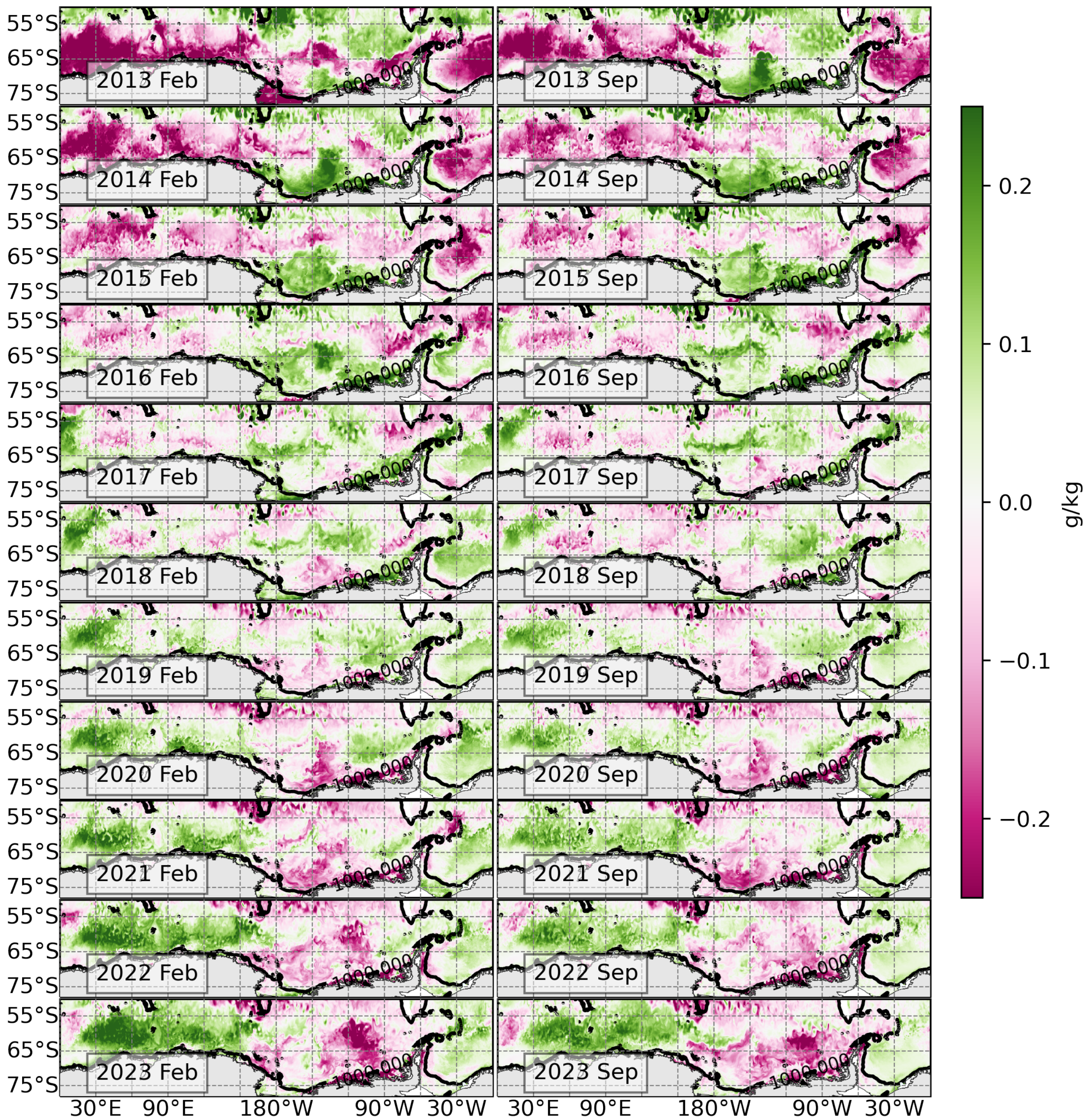

Figure S3: Upper-ocean (0 m to 100 m) salinity anomaly during February (left hand column) and September (right hand column).